

A dynamical mean-field theory approach to superconductivity and antiferromagnetism in a strongly correlated electron system .

H. Watanabe¹ and S. Doniach^{1,2}

Departments of Applied Physics¹ and Physics²
Stanford University, Stanford, CA 94305, U.S.A .

April 14, 2024

Abstract

In this paper, we present the results of numerical studies of superconductivity and antiferromagnetism in a strongly correlated electron system . To do this we construct a Hubbard model on a lattice of self-consistently embedded multi-site clusters (in practice two sites) by means of a dynamical mean-field theory in which intra-cluster dynamics is treated essentially exactly. We show that a class of characteristic features which have been seen in the excitation spectra of high- T_c cuprates including the pseudogap and the spin- χ resonance feature seen in neutron scattering studies, as well as their interplay with the onset of a pairing correlations, can be captured within a dynamical mean-field theory in which short-wavelength dynamics are rigorously treated. Thus we infer that the observation of the neutron scattering resonance in the superconducting state of the cuprate superconductors does not appear to be directly tied to their quasi-2D character.

Although our approach is defined strictly in terms of fermion degrees of freedom, we show that we can readily identify the emergence of effective low energy

bosonic degrees of freedom in the presence of a well-defined broken symmetry phase as long as their dynamics are dominated by short-range, short-wavelength fluctuations. Our exact calculations reveal that the dynamics of the spin degrees of freedom and the onset of superconductivity are strongly entangled. In particular, the dynamics of staggered spin degrees of freedom builds up coherence and a resonance-like sharp feature as superconducting pairing correlations set in (this feature diminishes in the normal phase). At the same time a spin gap develops in the staggered spin susceptibility. Under conditions of superconducting broken symmetry our approach thus extends static BCS mean field theory to provide an exact treatment of quantum fluctuations of the BCS order parameter within self-consistent dynamical mean-field theory. We find that both equilibrium and dynamical properties of our model can provide a consistent interpretation of experimental observations.

I. INTRODUCTION

Understanding the physics of strongly correlated electron systems has been one of the most difficult challenges in condensed matter physics for several decades. The importance of electron-electron correlations in high- T_c superconductors was recognized [1] soon after its discovery and much progress has been made in understanding its phenomenology. As a result of intensive efforts in both theoretical and experimental studies, the detailed nature of the microscopic mechanism for high- T_c is starting to become clearer and the idea that the superconducting instability is driven by Coulomb interactions is becoming more widely accepted, although it still remains controversial.

Besides undergoing a superconducting transition at high temperatures, the cuprate superconductors exhibit other features characteristic of strongly correlated systems including a pseudogap, spin fluctuation resonance, and non-Fermi liquid behavior in the normal state, some of which are also found in other transition metal oxides.

The key motivation of the present paper is to use an extended local dynamical mean field approach to study the effects of strong correlations on the superconducting instability. By going beyond the static mean field BCS treatment we are able to show

that coulomb correlations can stabilize the superconducting state and also lead to a relationship between the onset of superconductivity (or more generally, pairing fluctuations) and the spin dynamics similar to that seen experimentally. We are also able to study the onset of the pseudogap and its effects on the single particle properties of the system.

Considerable experimental evidence has accumulated which suggests that the microscopic pairing mechanism of high- T_c superconductivity may be already manifested at a relatively short length scale. Both superconducting coherence and spin-spin correlation lengths in high- T_c cuprates are relatively short. The in-plane superconducting coherence length, for example, is estimated to be roughly $\sim 15\text{\AA}$ which indicates that Cooper pairs, on average, span only a few lattice spacings. Also, the correlation length for spin degrees of freedom estimated from a relatively broad resonance peak width in a momentum space is also of the order of a few lattice spacings [2, 3, 4, 5, 6]. In addition, STM measurements of the influence of magnetic impurities on local electronic structure of high- T_c cuprates clearly suggest that Cooper pairs are local entities, and can exist in a microscopically confined region [7].

These measurements suggest that a theoretical description based on a real space representation (in contrast to the BCS momentum-space representation) in which fluctuations in a relatively localized region are rigorously treated can be a reasonable starting point to study the superconducting instability.

In this paper we show that a cluster-based dynamical mean-field theory approach is particularly useful for this purpose. Based on this approach, we are able to study the nature of short-ranged quantum fluctuations of a strongly correlated system in the presence of well-defined superconducting and antiferromagnetic broken symmetries.

The numerical results we report in this paper are an extension of earlier work [8] (unpublished) and are based on a Hubbard-like lattice model consisting of two-site clusters using the self-consistent dynamical mean-field theory approach of Kotliar and Georges [9]. In the dynamical mean-field theory approach, a lattice problem (for which an exact solution is generally difficult to obtain) is mapped onto an impurity problem coupled to an effective bath (which is typically much more tractable) – thus the advantage of this theory is that once the model is constructed it can be

solved in principle exactly without further approximations when supplemented by a self-consistency condition which is derived by requiring that the mean-field theory becomes exact in the $d \rightarrow \infty$ limit (d : dimension) [10]. The crucial point here is that the effective bath is allowed to be time-dependent and thus highly non-trivial quantum nature of (local) dynamics is retained. This approach has offered new insights to the physics of strongly correlated electron systems which are difficult to obtain from pre-existing theories [11].

Here, in order to address the quantum aspects of non-local but short-ranged fluctuations, we extend the original formalism to a self-consistent two-site cluster in order to be able to explore the superconducting part of the phase diagram. In order to treat superconductivity, we explicitly allow a $U(1)$ gauge symmetry breaking for both diagonal (on-site) [12] and off-diagonal (nearest-neighbor) [13] pairing channels inside a cluster. Within this model we are able to confirm the presence of a superconducting phase for reasonable Hubbard-type parameters. By virtue of enforcing self-consistency, our model effectively mimics an infinite system, and thus is able to sustain a generic symmetry breaking. Thus, our model facilitates a study of short-range fluctuations in a well-defined broken symmetry phase such as superconducting or Néel order.

Within this generalized model we are able to show that the onset of superconductivity is intimately coupled to antiferromagnetic spin fluctuations and that a resonance-like feature is indeed seen to emerge in the dynamical spin susceptibility as the superconducting order parameter switches on. Because we are able to solve the local cluster problem essentially exactly, the presence of the Hubbard on-site repulsion U will automatically favor an off-diagonal (nearest neighbor) superconducting order parameter over an on-site one. We interpret this by analogy with BCS mean-field theories of the cuprate superconductors [14, 15] as favoring a d -wave like as opposed to an s -wave like order parameter symmetry. Recently Lichtenstein and Katsnelson [13] and Maier et al [16] have developed approaches to dynamical cluster calculations for clusters with 4 or more sites which show properties similar to those found in our coupled 2-site model. Our calculations allow us to examine the spectra of excitations in our representation of the strongly correlated system which tie in well with experimental observations. The approaches of Lichtenstein and Katsnelson [13] and of Maier et al [16] may be expected to yield similar results. Recently, several groups

[17, 18] have argued that the resonance peak seen in inelastic neutron scattering may be thought of as a type of "spin-1p exciton". Our results suggest that the resonance is a generic property of the strongly coupled superconducting state and is not dependent on details of the cuprate band structure.

The following is the organization of the paper. Section II will describe the details of our methodology and technical aspects. In section III, we present our results as well as the interpretation. In section IV, we discuss the overall aspects of the results obtained in section III and also some issues which were not addressed in the preceding sections. We then suggest some future work and close the section with a summary. Supplemental derivations and discussions are given in appendices.

II. Methodology

A. Model and Formalism

A two-site cluster model is the minimal model needed to address the non-local nature of systems with order parameters for antiferromagnetism (staggered magnetization) and superconductivity (nearest-neighbor pairing) and we will base our analysis on this model (Fig.1). We retain on-site Coulomb repulsion U , intra-cluster hopping t^0 and inter-cluster hopping t . (The reason we distinguish inter-cluster from intra-cluster hopping will become clear below.) Thus, the physics which our model represents is described by the following partition function:

$$Z = \text{Tr} [e^{-H}]$$

$$H = \sum_{\langle i,j \rangle} t^X d_{A_i}^Y d_{B_j}^X + \sum_{(i,j)} t^0 d_{A_i}^Y d_{B_j}^X$$

$$+ \sum_i (d_{A_i}^X)^2 n_i^{\uparrow}$$

$$+ U \sum_i n_{A_i}^{\uparrow} n_{A_i}^{\downarrow} + U \sum_j n_{B_j}^{\uparrow} n_{B_j}^{\downarrow}$$

$$\begin{aligned}
& h_z \sum_i (\hat{n}_{A_i} - \hat{n}_{A_{i\#}}) + h_z \sum_j (\hat{n}_{B_j} - \hat{n}_{B_{j\#}}) \\
& + \sum_{\langle i;j \rangle} \hat{d}_{A_i}^y \hat{d}_{B_j}^y \\
& + (\mathbf{h} : \mathbf{c})
\end{aligned} \tag{1}$$

$$\tag{2}$$

where ϵ_d is a bare energy level of the d-orbital of our model (i.e., Cu $3d_{x^2-y^2}$ for high- T_c cuprates) and μ is a chemical potential. $\hat{d}_{A_i}^y$ is the creation operator of an electron with spin \uparrow on the i th site of the A sublattice. $\langle i;j \rangle$ and $(i;j)$ represent the sum over the inter and intra-cluster nearest neighbors, respectively. h_z is an infinitesimal staggered magnetic field. \mathbf{h} is an infinitesimal $U(1)$ gauge symmetry breaking field for ϕ -diagonal pairing, which we take to be real (and all the anomalous components as well).

Now, we self-consistently embed our cluster into a lattice. Although the details of energetics of charge and spin degrees of freedom may depend on the lattice, most of the qualitative physics which appear to be manifested in real systems are shared by the tight-binding Hubbard-like lattice models embedded on a lattice which has a bipartite nature and a relatively smooth, structureless DOS [19, 20, 21]. In this study, we chose to work with a Bethe lattice.

The self-consistency condition basically arises as a result of seeking a homogeneous solution in the lattice problem. Here, we essentially follow the prescription developed by Kotliar and Georges [11, 22] and extend it to the case of two-site clusters in the presence of superconductivity. The basic idea is to systematically expand (1) with respect to the inter-cluster hopping and pairing amplitude (scaled as $t = \frac{t}{\epsilon_d}$; $\phi = \frac{\phi}{\epsilon_d}$) and integrate out over the ligand degrees of freedom. Due to the above scaling, to order $O(1)$, only the lowest order term (the two-point propagator of the ligand multiplied by the probing fields) survives the integration and we obtain the following mean-field partition function

$$Z_{MF} = \int_{\text{local}} \prod_D \hat{D}^y e^{S_{\text{eff}}} \tag{3}$$

where

$$S_{\text{eff}} = \sum_{\mathbf{Z}} \sum_{\mathbf{Z}'} d_{\mathbf{Z}} d_{\mathbf{Z}'} \hat{G}_o^{-1}(\mathbf{Z}, \mathbf{Z}') \hat{\psi}(\mathbf{Z}) \hat{\psi}(\mathbf{Z}') + \sum_{\mathbf{Z}} U_{\mathbf{Z}} d_{\mathbf{Z}} \left(\hat{n}_{A\#}(\mathbf{Z}) - \frac{1}{2} \right) \left(\hat{n}_{A\#}(\mathbf{Z}) - \frac{1}{2} \right) + \sum_{\mathbf{Z}} U_{\mathbf{Z}} d_{\mathbf{Z}} \left(\hat{n}_{B\#}(\mathbf{Z}) - \frac{1}{2} \right) \left(\hat{n}_{B\#}(\mathbf{Z}) - \frac{1}{2} \right)$$

$\hat{\psi} = (\hat{d}_{A\#}^{\uparrow}, \hat{d}_{B\#}^{\uparrow}, \hat{d}_{A\#}^{\downarrow}, \hat{d}_{B\#}^{\downarrow})$ is a four-component Nambu-Gorkov spinor representing the local degrees of freedom. \hat{G}_o is a 4 × 4 cavity propagator for the cluster which can be thought of as a local noninteracting propagator of a particular cluster where only the on-site U for this cluster is turned off but all the other U are still present. From the above effective local action, a total propagator G() can be calculated as:

$$\hat{G}(\mathbf{Z}, \mathbf{Z}') = \frac{\int_{\text{local}} \mathcal{D} \hat{\psi} \hat{D} \hat{\psi} \hat{\psi}(\mathbf{Z}) \hat{\psi}(\mathbf{Z}') e^{S_{\text{eff}}}}{Z_{\text{MF}}} \tag{4}$$

Once a total propagator is obtained, the cavity propagator in the Bethe lattice case is then given through the following self-consistency condition which can be conveniently expressed in frequency space:

$$G_o^{-1}(\mathbf{i}!_n) = \begin{pmatrix} D_{AA}^{\uparrow\uparrow}(\mathbf{i}!_n) & D_{AB}^{\uparrow\uparrow}(\mathbf{i}!_n) & A_{AA}^{\uparrow\#}(\mathbf{i}!_n) & A_{AB}^{\uparrow\#}(\mathbf{i}!_n) \\ D_{BA}^{\uparrow\uparrow}(\mathbf{i}!_n) & D_{BB}^{\uparrow\uparrow}(\mathbf{i}!_n) & A_{BA}^{\uparrow\#}(\mathbf{i}!_n) & A_{BB}^{\uparrow\#}(\mathbf{i}!_n) \\ A_{AA}^{\#\uparrow}(\mathbf{i}!_n) & A_{AB}^{\#\uparrow}(\mathbf{i}!_n) & D_{AA}^{\#\#}(\mathbf{i}!_n) & D_{AB}^{\#\#}(\mathbf{i}!_n) \\ A_{BA}^{\#\uparrow}(\mathbf{i}!_n) & A_{BB}^{\#\uparrow}(\mathbf{i}!_n) & D_{BA}^{\#\#}(\mathbf{i}!_n) & D_{BB}^{\#\#}(\mathbf{i}!_n) \end{pmatrix}$$

where

$$D_{AA}^{\uparrow\uparrow}(\mathbf{i}!_n) = \mathbf{i}!_n d + \frac{U}{2} t^2 G_{BB}^{\uparrow\uparrow}(\mathbf{i}!_n);$$

$$A_{AA}^{\uparrow\#}(\mathbf{i}!_n) = t^2 F_{BB}^{\#\uparrow}(\mathbf{i}!_n);$$

$$D_{AB}^{''''} (i!_n) = t^0 t^2 G_{BA}^{''''} (i!_n);$$

and similarly for the other elements of G_o^{-1} . Full expressions are given in the Appendix.

A few comments are in order. As a result of the decomposition of the lattice into clusters and treating the physics inside and outside the clusters in a different fashion (see, however, [23, 24]), the ratio of the bare values of the inter- and intra-cluster hopping matrix elements no longer reflects the actual physics so that they should not be compared directly. Here, our main focus is on the short-range superconducting and antiferromagnetic spin fluctuations; i.e. that at part of the physics which intrinsically depends on the short-range dynamics, should not depend qualitatively on the construction of the lattice, and should still be manifested in the intra-cluster dynamics. Considering the overall qualitative consistency of our results with experiments (please see Sec.III), we believe that the physics presented here is not an artifact due to the specific construction of our model.

As will be shown below (see results) the self consistent numerical solution of the above model leads to a phase diagram exhibiting both antiferromagnetism and superconductivity. However, we find that the superconducting critical temperature is relatively low for us to be able to obtain reliable numerical results for the excitation spectrum of the model. In order to strengthen the tendency of the model to go superconducting, we perform a heuristic extension of the cluster expansion of the lattice action to higher orders in $\frac{1}{d}$ and incorporate the effect of inter-cluster particle-particle correlations. For example, at $O(\frac{1}{d})$, by employing the idea of the Hartree-Fock theory, we can extract a inter-cluster particle-particle correlation from the following four-point propagators in a local effective action S_{eff} :

$$\sum_{i_0}^Z \sum_{i_1}^Z \sum_{i_2}^Z \sum_{i_3}^Z d_{i_1} d_{i_2} d_{i_3} d_{i_4} \hat{d}_{oA}^x(i_1) \hat{d}_{oB}^y(i_2) \hat{d}_{oA}^x(i_3) \hat{d}_{oB}^y(i_4) \hat{G}_{BABA}^{''''''} (i_1 i_2 i_3 i_4)$$

$$\mathcal{F}(0) \int_{i_0}^Z \int_{i_1}^Z d_{i_1} d_{i_2} \hat{d}_{oA}^y(i_1) \hat{d}_{oB}^x(i_2) \hat{d}_B^y(i_1) \hat{d}_A^x(i_2)$$

$$+ \overline{f(0)} \sum_0^Z \sum_0^Z d_{12} d_{oB\#(1)} \hat{d}_{oA\#(2)} \hat{d}_{A\#(1)} \hat{d}_{B\#(2)}$$

where $\overline{f(0)}$ is the average of equal-time inter-cluster anomalous Green's function. \hat{d}_{oA}^Y and \hat{d}_A^Y represent local and neighboring cluster degrees of freedom respectively. In the above, since each local degree of freedom carries a pre-factor $\frac{1}{d}$ and we sum it over all d nearest neighbors, the above term becomes the order of $O(\frac{1}{d})$.

We then incorporate the inter-cluster pairing correlation from higher orders in $\frac{1}{d}$ by employing the idea of the BCS theory. In order to preserve the effects of translational invariance within the Bethe lattice model, we then substitute the inter-cluster pairing by the intra-cluster pairing correlations which can be rigorously calculated :

$$\begin{aligned} & g_{(i,j);}^{inter X} \hat{d}_{oA_i}^Y \hat{d}_{B_j}^Y \hat{d}_{B_j} \hat{d}_{oA_i} \\ & , \quad g_{(i,j);}^{inter X} \langle \hat{d}_{oA_i}^Y \hat{d}_{B_j}^Y \rangle \hat{d}_{B_j} \hat{d}_{oA_i} + g_{(i,j);}^{inter X} \hat{d}_{oA_i}^Y \hat{d}_{B_j}^Y \langle \hat{d}_{B_j} \hat{d}_{oA_i} \rangle \\ & , \quad g_{(i,j);}^{inter X} \langle \hat{d}_{oA_i}^Y \hat{d}_{oB_j}^Y \rangle \hat{d}_{B_j} \hat{d}_{A_i} + g_{(i,j);_1}^{inter X} \hat{d}_{A_i}^Y \hat{d}_{B_j}^Y \langle \hat{d}_{oB_j} \hat{d}_{oA_i} \rangle \\ & g_{(i,j);}^{inter @} \sum_{AB} \hat{d}_{B_j} \hat{d}_{A_i} + \sum_{(i,j);} \hat{d}_{A_i}^Y \hat{d}_{B_j}^Y \sum_{BA} \hat{d}_{BA} \end{aligned}$$

where $\langle \hat{d}_{oA_i}^Y \hat{d}_{oB_j}^Y \rangle_{AB}$ is the thermal average of instantaneous intra-cluster pairing which is calculated from the local quantum dynamics. For simplicity inter-cluster and intra-cluster coupling constants are taken to be the same, $g^{intra} = g^{inter}$ and we set their value equal to t . We then take a mean-field limit with respect to the inter-cluster hopping matrix elements as well, i.e., $\hat{d}_{ij} = \frac{1}{d}$, and obtain the following equations:

$$\begin{aligned}
D_{AA}^{\prime\prime\prime}(\mathbf{i}!_n) &= \mathbf{i}!_n \quad d + \quad + h_z \quad \frac{U}{2} \quad t^2 G_{BB}^{\prime\prime\prime}(\mathbf{i}!_n) \\
&\quad t^2 \quad \begin{matrix} \prime\prime \\ AB \end{matrix} \quad \begin{matrix} \prime\prime \\ BA \end{matrix} \quad G_{BB}^{\prime\prime\prime}(\mathbf{i}!_n) \\
&\quad t^2 \left(\begin{matrix} \prime\prime \\ AB \end{matrix} F_{BB}^{\prime\prime}(\mathbf{i}!_n) + \begin{matrix} \prime\prime \\ BA \end{matrix} F_{BB}^{\prime\prime}(\mathbf{i}!_n) \right);
\end{aligned}
\tag{5}$$

$$\begin{aligned}
A_{AA}^{\prime\prime}(\mathbf{i}!_n) &= t^2 F_{BB}^{\prime\prime}(\mathbf{i}!_n) \\
&\quad t^2 \quad \begin{matrix} \prime\prime \\ AB \end{matrix} \quad \begin{matrix} \prime\prime \\ BA \end{matrix} \quad F_{BB}^{\prime\prime}(\mathbf{i}!_n) \\
&\quad + \quad t^2 \left(\begin{matrix} \prime\prime \\ AB \end{matrix} G_{BB}^{\prime\prime\prime}(\mathbf{i}!_n) \quad \begin{matrix} \prime\prime \\ BA \end{matrix} G_{BB}^{\prime\prime\prime}(\mathbf{i}!_n) \right); \\
&\quad \text{etc}
\end{aligned}
\tag{6}$$

where only representative components are shown and the full expressions are given in the Appendix.

We will see that the effects of the additional inter-cluster coupling are manifested in all the components of the propagator. As we show in section III, superconductivity already appears in the absence of inter-cluster pairing correlations. When the additional inter-cluster coupling is included we find as expected that the inter-cluster coupling stabilizes the superconducting phase. In particular, T_c is enhanced for all the doping levels and the single-particle gap (i.e., the superconducting gap) becomes more pronounced. This enhancement in turn enables us to perform computations at higher temperature and hence to obtain more detailed excitation spectra in the superconducting region of the phase diagram.

B. Numerics

The local dynamics (3) and (4) is basically that of a degenerate impurity Anderson model (with the $U(1)$ gauge symmetry breaking) and can be solved in various ways. Here, we chose to solve it numerically using the quantum monte carlo (QMC) algorithm of Hirsch and Fye [25]. Since there are two vertices in the local action (3), two Ising variables are introduced in our case. Then importance sampling is performed sequentially based on the ratio of the statistical weights for flipping Ising variables, which are given by [8]:

$$\begin{aligned}
R_A(i) &= ((e^{A(i)} - e^{-A(i)})G_{AA}'''(i; i) + e^{A(i)}) \\
&\quad ((e^{A(i)} - e^{-A(i)})G_{AA}^{##}(i; i) + e^{A(i)}) \\
&\quad (e^{A(i)} - e^{-A(i)})^2 F_{AA}^{##}(i; i) F_{AA}^{##}(i; i) \\
R_B(i) &= ((e^{B(i)} - e^{-B(i)})G_{BB}'''(i; i) + e^{B(i)}) \\
&\quad ((e^{B(i)} - e^{-B(i)})G_{BB}^{##}(i; i) + e^{B(i)}) \\
&\quad (e^{B(i)} - e^{-B(i)})^2 F_{BB}^{##}(i; i) F_{BB}^{##}(i; i)
\end{aligned}$$

where $A_{(B)}(i)$ is the Ising variable at a time step i ($i=1, \dots, L$; L : the number of time slices) which is introduced to decouple the Hubbard U term of A (B) site in a cluster. Here, we would like to warn the reader not to confuse Ising variables with electron spins. Ising variables are basically the fluctuating fictitious magnetic field which couple to electron spins. β is a constant which is given by the relation, $\cosh(\beta) = e^{\frac{U}{2T}}$. $G_{AA}'''(i; i)$ is a diagonal component (in terms of imaginary time index) of the instantaneous Matsubara Green's function at time step i of an arbitrary sweep, and should not be confused with the averaged Matsubara Green's function defined in (4). If the spin at the time slice k is accepted, each component of the Matsubara Green's functions is updated according to the following rule:

$$\begin{aligned}
\hat{G}_{ab}^{\text{new}}(i; j) &= \hat{G}_{ab}^{\text{old}}(i; j) \\
&+ \sum_c \frac{(\hat{G}_{ac}^{\text{old}}(i; k) - \hat{G}_{ac}^{\text{old}}(i; k)) (e^{V_{cc}(k)} - 1)}{1 + (1 - \hat{G}_{cc}^{\text{old}}(k; k)) (e^{V_{cc}(k)} - 1)} \hat{G}_{cb}^{\text{old}}(k; j)
\end{aligned} \tag{7}$$

$$\begin{aligned}
V_{ab}(i) &= 2 A(i) \mathcal{A} \langle A \rangle < A \rangle j \\
&2 A(i) \mathcal{A} \langle A \rangle < A \rangle \# j \\
&2 B(i) \mathcal{B} \langle B \rangle < B \rangle j \\
&2 B(i) \mathcal{B} \langle B \rangle < B \rangle \# j
\end{aligned}$$

$$\begin{aligned}
a_i b_j c_k &= f_A \delta_{ij} \delta_{jk} + f_B \delta_{ij} \delta_{ik} + f_C \delta_{ij} \delta_{ik} \\
i, j, k &= 1, \dots, L
\end{aligned}$$

where $V_{ab}(i)$ is a diagonal tensor which represents the amount of change in the action associated with the flip of an Ising variable at time slice i .

The above set of equations (3)–(5) is iterated until the convergence is achieved. In practice, a particular form of starting propagator is guessed depending on the type of the anticipated solution. The impurity problem (3) and (4) might be solved more efficiently by combining exact diagonalization and a Padé approximation [11]. The energy resolution of this approach basically depends on the number of energy levels to be used as a basis. Thus, it may not be the best approach when the spectral weight is widely spread and a tiny feature is under search (such as a dip structure in the ARPES spectrum in this case. Please see Section 8.2). Probably, this approach is best used when the shape of the spectral function is qualitatively known or reasonably guessed.

A few remarks are in order regarding the sampling algorithm. A complete algorithm would be to integrate over the entire phase space of $\phi_A(i)$ and $\phi_B(j)$ ($i, j = 1, 2, \dots, L_A$). The size of the entire phase is $2^{L_A} 2^{L_B}$ and it will be impractical to sample all the configurations for most of the temperatures studied. This can then be dealt with by importance sampling. However, with this algorithm, we encountered a negative sign problem at the lowest temperature studied ($T = 96$) for finite doping, and for higher temperatures, although the SDW persists for finite doping, we found no sign of development of a gap in the single-particle spectra, and no sign of the onset of or spin gap or building up of coherence in a staggered spin susceptibility, and no sign of the onset of superconductivity. This phase basically corresponds to an antiferromagnetic metal. In the DMFT based formalism, a metal-insulator transition is described as the onset of local or short-ranged gapless single-particle excitations and in this case, the transition is driven by carrier doping and accompanied by antiferromagnetic order.[27]

Since our primary goal is to investigate the relationship between short-ranged antiferromagnetic spin fluctuations and superconductivity, we took a slightly different approach. The idea is to implement an algorithm such that once the system starts to build up an AF correlation (indicated by the appearance of a SDW as mentioned

above), two Ising variables are biased to stay at staggered configurations, namely (";#) or (#;"). In other words, we attempt to build a machinery to do algorithmic projection onto low-lying states. One way to implement this idea is to use an identical random number array for both the A and B sublattices. More specifically, we first attempt a flip of $A(i)$ and see if $R_A(i) > x_i$ (random number) to accept the flip and update. Subsequently, we do the same for the B-site using the same random number x_i . The motivation for this algorithm is basically a sublattice symmetry of our model which is manifested in the expressions for the accept ratio (please see the appendix for more details), i.e.,

$$R_A(i) = R_B(i) \Big|_{B=A; A, B; ", \#} \tag{8}$$

Once the system passes into an antiferromagnetically correlated critical domain (by which we mean a domain where the system acquires a tendency to pick staggered configurations), the flip which causes a transition from a parallel to a staggered configuration starts to get accepted more frequently than the flip which causes the opposite transition. For the sake of argument, let us consider the idealized case in which the former flip is always accepted (that is to say, accept ratio for the former flip is always greater than 1. Although this is generally not true due to the presence of fluctuations, the argument below can be easily generalized to a more realistic case).

Suppose the Ising variables for A and B sublattices are initially in the $(A; B) = (";#)$ configuration at $t = t_i$. Then, due to the sublattice symmetry, if the flip of A is not accepted, the flip of B is not likely to be accepted either, i.e., if $R_A(i) < x_i$ for the flip $(A; B) : (";#) \rightarrow (\#;#)$, then, it is likely that $R_B(i) < x_i$ for the flip $(A; B) : (";#) \rightarrow (";")$ as well due to the sublattice symmetry. That is, if the initial configuration is a staggered one, a conditional probability that a B flip is not accepted given that a A flip is not accepted is high. This, of course, depends on the level of noise, thermal or quantum, already present, that is, the above statement holds in an averaged sense. The better a sublattice symmetry is preserved at each time slice, the stronger this correlation will be. Please note that if we use a random number y_i for the determination of a flip of B which is completely uncorrelated with x_i , then the probability of a B flip solely depends on the value of $R_B(i)$ and a rejection of A flip has no bearing on the B flip. If the flip of A is accepted and the system is updated

to (#;#) configuration, due to the presence of antiferromagnetic correlation, the flip of B will always be accepted (as assumed above). Therefore, in this case, whether or not to use the same random number will have no influence on the statistics.

If the initial configuration is a parallel one, say, $(A; B) = (";")$, then due to the presence of antiferromagnetic correlation, a flip of A will always be accepted and the system is updated to (#;"). Therefore, in this case, it will make no difference whether or not to use the same random number for the flip of B . Thus, our algorithm is expected to bias the system towards staggered configurations more than a standard algorithm, when a system acquires an antiferromagnetic correlation. The above argument can be easily generalized to the case where antiferromagnetic correlations are not ideal, i.e., the probability of a flip from a parallel to a staggered configuration is less than 1.

Please note that, once the system starts to lose antiferromagnetic correlations (by which we mean that the transition probability between staggered and parallel configurations becomes equal), then the final population of the two configurations will converge to the same value. At this stage the effects of our algorithm will also start to diminish, simply because transitions from a staggered to parallel configuration become more frequent and the conditional probability discussed above becomes irrelevant. Therefore our algorithm more or less approaches the standard Metropolis-style algorithm when the antiferromagnetic correlation diminishes, but starts to deviate from it when the system passes into an antiferromagnetically correlated phase. (Our algorithm respects spin rotational symmetry in the paramagnetic phase.) Please note that in our algorithm Ising variables can in principle take all possible configurations and no symmetry on the state is explicitly enforced. Therefore the symmetry and dynamics of the system still depends on the physics and remain nontrivial.

As will be seen from results in Sec.III, our algorithm leads to the onset of coherent antiferromagnetic spin fluctuations for a certain parameter regime and unambiguously identifies a close tie between the onset of SC and of a coherent antiferromagnetic spin fluctuation. We will see that the results obtained by our algorithm, both for the dynamical and equilibrium properties of the model, are qualitatively consistent with the experimental findings for high- T_c cuprates. This suggests that the spin dynamics and its relation to the onset of superconductivity as found with our algorithm is more

or less consistent with what is realized in real systems.

Once the imaginary-time correlation functions are evaluated, equilibrium quantities can be directly calculated from the self-consistent Matsubara Green's functions, and dynamical quantities can be obtained from the via analytic continuation. We employed the Maximum Entropy (ME) [29, 28] method to do this. For each set of parameters, we perform the iteration (3)–(5) and (7) until all the main features in the dynamical spectrum converge. In this study, we chose the number of time slices, L , to be such that $\frac{1}{L} = 0.25$ which should be sufficiently small to obtain a reliable value for the physical quantities of interest. [30].

III. Results and Discussion

A. Choice of Parameters

We choose $t = 0.5$ throughout this paper such that the bare bandwidth of the underlying Bethe lattice (equal to $2t$) is the unit of the energy scale. $U = 2.2$ was chosen based on a preliminary study on the one-band Hubbard model where we found this makes the Neel temperature roughly optimal at half-filling. Then we sampled a few t^0 values to search for the one which leads to a Neel state with the experimentally observed $\langle S_z \rangle = (0.5 \mu_B)$ at half-filling. The optimal value for t^0 appears to be located somewhere between 0.1 and 0.2. In this paper, we show the results for $t^0 = 0.2$. (Setting $t^0 = 0.1$ does not modify the results in a qualitative way.) Although the above parameter setting has not been carefully adjusted to be the optimal choice, the overall agreement (qualitative and quantitative) with the experimental findings suggests that the above set of values are reasonable to reflect those for real materials. Again, let us emphasize here that our main interest is to study the qualitative relationship between superconductivity and antiferromagnetism.

B . Single-particle spectra

We will present single-particle spectra both with and without the inter-cluster pairing coupling, and also compare them in the normal and superconducting phases. The single-particle spectra are defined as follows:

$$\begin{aligned} G(\omega) &= \text{Im Tr} \hat{G}(i\omega) \\ &= G_{AA}^{\text{""}}(\omega) + G_{AA}^{\text{##}}(\omega) + G_{BB}^{\text{""}}(\omega) + G_{BB}^{\text{##}}(\omega) \end{aligned} \quad (9)$$

Fig.2 shows the results at $\delta = 0.6$ ($\delta = 0.05$) and $\delta = 0.3$ ($\delta = 0.17$) without the inter-cluster pairing coupling. Superconductivity sets in at $T_c = 16$ for both dopings. The onset of superconductivity is determined by the onset of the average of the equal-time anomalous Green's function which is defined as:

$$\mathcal{F}(\omega) = \mathcal{F}_{AB}^{\text{""}}(\omega) + \mathcal{F}_{BA}^{\text{##}}(\omega) + \mathcal{F}_{AB}^{\text{##}}(\omega) + \mathcal{F}_{BA}^{\text{""}}(\omega)$$

A single-particle gap starts to form when superconductivity sets in and a quasiparticle-like feature appears on top of the valence band as the temperature is lowered. Also, a dip which separates the quasiparticle peak and the relatively broad feature develops.

Next, we study the case with inter-cluster coupling included where we have assumed $g^{\text{intra}} = g^{\text{inter}}$. As discussed above, this heuristic extension of our 2-site cluster model is put in to give a more robust superconducting ground state, which allows us to extend our numerical calculations over a wider temperature range for studying the properties of the superconducting state. Fig.3 shows a normal state single-particle spectrum for $\delta = 0.05$ and $T_c = 16$ which was obtained by setting all the anomalous components of the Green's function to zero (i.e., $\mathcal{F} = 0$). We confirmed that superconductivity indeed develops at this parameter setting when the anomalous components are turned on. As we notice, in the absence of these components, the single-particle gap disappears and a sharp Kondo-like peak develops at the Fermi level, indicating that holes which participate in the pairing are strongly correlated. Fig.4 shows the effect of inter-cluster pairing on the evolution of single-particle Green's function as a function of temperature for $\delta = 0.7$ ($\delta = 0.04$) and $\delta = 0.3$ ($\delta = 0.17$) where we have adopted the above values for t^0 and U for which g is as shown above. Although the overall features are similar to Fig.2, T_c is increased (superconductivity sets in at

10) and the single-particle gap becomes more robust especially at smaller doping. Experimentally, a single-particle gap has been found to decrease as a function of doping [32].

In all the cases shown above, superconductivity is found to set in before a robust gap has been formed (In particular, for $\mu = 0.3$ with inter-cluster pairing). As we will show later, a signature of the onset of pairing fluctuations is more visible in the pair-pair correlation function. The onset of pairing fluctuations despite the absence of a robust gap is basically due to fluctuation effects which are neglected in the BCS mean-field theory. Here we are able to see this effect through our use of the dynamical mean-field theory approach. In order to confirm that the gap formation is due to the onset of superconductivity, we also studied the single-particle spectra in the normal state for the same parameter settings. Fig.5 shows single-particle spectra at fixed doping ($\mu = 0.04$) as a function of temperature in the normal state. A "Kondo peak" is manifested in the spectra [20]. For visual assistance, we overlay the results already shown in Fig.5 (a) for the superconducting state. As the superconducting amplitude grows, the spectral weight near ϵ_F is depleted and transferred to the gap edges. These results unambiguously show that the single-particle gap is driven by the onset of superconductivity. Fig.6 shows the single-particle gap (determined by the FM HW), T_c , and $\langle j^2(0) \rangle$ (please see Sec.III(D)) as a function of doping at $\mu = 16$. Except for the low doping region, $\epsilon_{1\text{particle}}$ roughly scales as T_c , which is what one would expect in the BCS picture.

Next we compare our results with the ARPES data. Since the single-particle spectra calculated here are local, they should be in principle interpreted as angle-integrated quantities. Thus, only a qualitative comparison can be made with the angle resolved data. First, the quasiparticle peak as well as the dip for both doping is qualitatively consistent with the ARPES measurements. By comparing the spectra for the normal phase with those for the superconducting phase, the appearance of the quasiparticle peak in the superconducting phase can be qualitatively understood within the BCS picture in which quasiparticles in the vicinity of ϵ_F ($j = \epsilon_F$ $\epsilon_{1\text{particle}}$) in the normal phase form the Cooper pairs and the quasiparticle peaks appear at both gap edges. The appearance of the dip implies the separation of two energy scales, a sharp feature closer to ϵ_F and a broad feature below the sharp one. This broad feature is quite reminiscent of the "hump" which has been observed in the ARPES measurements.

Recently, the microscopic origin of the "hump" has been debated [34, 33], and argued that the underlying band structure of high- T_c cuprates is important for the onset of hump [33]. Here, we would like to make some remarks on this issue based on the results of our calculation. As shown above, the appearance of the hump is strongly correlated with the onset of superconductivity (or a quasiparticle peak). As we show later, a short-range antiferromagnetic spin fluctuation emerges as a coherent mode as superconductivity sets in. (Please note that our calculation is essentially exact and considers all energy scales involved). Therefore, it is reasonable to suspect that a hump-like feature is due to scattering of the photoelectrons by these coherent antiferromagnetic spin fluctuations. In fact, the separation of the quasiparticle peak and the hump-like feature is roughly proportional to the characteristic frequency of the antiferromagnetic spin fluctuations. This is an indication that the appearance of the two energy scales is due to a resonance. Please also note that since our calculation is fairly local, our results suggest that a peak-dip-hump feature seen in ARPES measurements does not depend on the details of the underlying band structure.

The evolution of the single-particle gap as a function of doping is also consistent with the ARPES experiments [35, 32, 36] in which a pseudogap was found to monotonically decrease in the underdoped region and fall off more rapidly in the overdoped region as the doping increases. This suggests that T_c obtained in this study behaves more like T^* . This observation is also consistent with the above finding that single-particle spectra start to show an anomaly at T_c . The actual ARPES spectra show a more pronounced quasiparticle peak than the one found here. This could be due to the fact that our DOS is an angle-integrated quantity and is also limited by the resolution of the Maximum Entropy algorithm.

C. Two-Particle Correlation functions

When a gap develops in a single-particle channel, a coherence or rigidity usually start to build up in two-particle channels. A natural question is then if and how two-particle correlation functions show anomalous behavior as a result of the onset of superconductivity. This question is also motivated by the fact that the pseudogap has been observed in ARPES, ETM and STM (which basically measure single-particle spectra) and that INS, NMR and transport measurements (which basically probe the two-particle correlation functions in spin and charge sectors) have also found rich phe-

nom ena as the pseudogap sets in. In this section, we present local susceptibilities of relevant bosonic degrees of freedom (both particle-hole and particle-particle channel) which appear to be playing an important role in high- T_c cuprates.

1. Spin degrees of freedom

Experimental studies of spin dynamics have been one of the most valuable source of information on the microscopics of high- T_c cuprates. In this section, we particularly focus on resonance and a spin-gap features, and their relation to superconductivity. The onset of the resonance which has been observed in inelastic neutron scattering (INS) measurements as a narrow peak at the antiferromagnetic wave vector $Q = (\frac{\pi}{a}; \frac{\pi}{a})$ (a lattice parameter) and energy ~ 41 meV (near the optimal doping) [37, 38, 39, 40], seems to be intimately related to the onset of superconductivity [40, 5]. The microscopic origin of this resonance as well as its connection to the onset of superconductivity has been recently debated by a number of authors [17, 18, 53]. The spin gap is characterized by a depletion of low energy spectral weight in the dynamical spin susceptibility at commensurate wave vector Q and its onset appears to be correlated with that of a single-particle gap in ARPES spectrum [5]. The relevant quantity is the dynamic staggered spin susceptibility $\chi_z(Q; \omega)$ which basically contains the information about the collective excitations of spin degrees of freedom at wave vector Q . Using linear response theory, $\chi_z(Q; \omega)$ is given as the following retarded staggered spin-spin correlation function:

$$\chi_z(Q; \omega) = i \int_0^{\infty} dt e^{i\omega t} \langle [\hat{M}_z(t); \hat{M}_z(0)] \rangle$$

where the staggered magnetization in our two-site cluster is defined as:

$$\begin{aligned} \hat{M}_z(t) &= \hat{S}_z^A(t) - \hat{S}_z^B(t) \\ &= (\hat{n}_{A\uparrow}(t) - \hat{n}_{A\downarrow}(t)) - (\hat{n}_{B\uparrow}(t) - \hat{n}_{B\downarrow}(t)) \end{aligned}$$

Then, by the fluctuation-dissipation theorem and analytic continuation, $\chi_z(Q; \omega)$ can be directly calculated from the imaginary-time staggered spin-spin correlation func-

tion which is given as:

$$S_z(Q; \omega) = \frac{\langle \hat{M}_z(Q, \omega) \hat{M}_z(Q, 0) \rangle}{Z_{MF}}$$

$$= \frac{\text{Tr} \left[\hat{D}^{\text{local}} \hat{D}^{\text{D}} \hat{M}_z(Q, \omega) \hat{M}_z(Q, 0) e^{-S_{\text{eff}}} \right]}{Z_{MF}}$$

The dynamic spin susceptibility, $\chi_z(Q; \omega)$ can then be calculated using the fluctuation-dissipation theorem as follows:

$$\chi_z(Q; \omega) = (1 - e^{-\beta \hbar \omega}) S_z(Q; \omega)$$

Please see the appendix for more details of the calculation.

One remark should be made here. $\chi_z(Q; \omega)$ defined above should be interpreted as a measure of short-range fluctuations (i.e. the relevant length scale represented by the clustering) due to the two-site cluster nature of the model. That is, the above $\chi_z(Q; \omega)$ is a response function defined for a probing field which acts only on the two sites in our cluster instead of the entire lattice. Thus, when Néel order sets in and the spin-spin correlation length becomes sufficiently longer than the cluster size, $\chi_z(Q; \omega)$ will start to deviate from the global staggered susceptibility defined as a response function of the entire lattice. Although we will not have precise information on the correlation length until we actually calculate it (probably by gradually increasing the cluster size which will become numerically expensive as mentioned above and is beyond the scope of this paper). Since a well-defined SDW is severely degraded as soon as the system is doped, and as mentioned earlier, the correlation length of spin fluctuations in high- T_c cuprates away from half-filling as estimated by neutron scattering measurements is roughly of the order of a few lattice spacing, we believe that the local description given above should be a reasonable approximation.

Fig.7 and 8 show the evolution of $\chi_z(Q; \omega)$ as a function of temperature for different doping levels with and without inter-cluster pairing. In all cases, as the temperature is reduced, a feature starts to grow at some energy scale and becomes more coherent at lower temperatures. At the same time, low energy spectral weight is

gradually depleted and the spectrum eventually becomes gapped. These features are quite reminiscent of the observed behavior of the resonance and spin gap. Since the superconductivity starts to set in at $t = 10$ with inter-cluster coupling and at $t = 16$ without it, they appear to be correlated with the onset of superconductivity. The position of the resonance appears to be rather insensitive to temperature variation. Next, we plot $\chi_z(Q; \omega)$ as a function of doping at $t = 16$ for no inter-cluster coupling (Fig.9 (a)) and with inter-cluster coupling (Fig.9 (b)). As long as superconductivity persists, a peak basically remains visible. The position of the peak appears to increase monotonically as a function of doping, and as a result, the spin gap also increases as the doping is increased (at least in the underdoped region). Upon passing into the overdoped region, the peak suddenly becomes incoherent and the spin gap disappears. We also found that where a resonance remains coherent, its energy is basically below a particle-hole continuum (i.e., $\omega_{res} < 2\epsilon_{sc}$. See below for optical conductivity results). The overall qualitative feature of the evolution of $\chi_z(Q; \omega)$ as a function of doping is basically similar for both cases.

Now we compare the above results with the experiments. A resonance peak has been found by spin-polarized INS in the superconducting phase [40, 5, 3]. The position of resonance ω_{res} has been observed to soften as the doping is decreased from the optimal level [2, 5, 41] and appears to be relatively temperature insensitive [3, 5, 42, 43] for a fixed doping. The magnitude of a spin gap also appears to decrease as the doping is reduced from optimal doping [5, 3]. These features are also qualitatively captured by our results. Furthermore, the relative energy scales among the resonance, spin gap and single-particle gap as found by INS and ARPES measurements are semi-quantitatively consistent with the results shown in Fig.4, Fig.5, Fig.7 and Fig.8.

To further investigate the relation of the spin spectra with superconductivity, we also studied the spectra in the normal phase. Fig.10 is $\chi_z(Q; \omega)$ for $t = 16$ and $t = 0.17$. For comparison, we also show the data in the superconducting phase with roughly the same parameter settings. In the normal phase, the coherence of the resonance is severely degraded and the existence of the peak can no longer be recognized. Also, $\chi_z(Q; \omega)$ acquires a substantial weight in the low energy sectors and the spin gap is completely filled up. These findings imply that the short-range antiferromagnetic spin fluctuations maintain their coherence by means of the pairing correlations.

2. Charge degrees of freedom Next, we present the dynamics of charge degrees of freedom. Since all the qualitative features found for the case of no inter-cluster pairing are also found when the inter-cluster pairing is switched on, we will only show the results for the latter case. Optical measurements have also revealed the emergence of a gap feature at some temperature T which is higher than T_c in the underdoped region. A relevant physical quantity which probes the charge dynamics is the optical conductivity which is directly related to the retarded current-current correlation function. In our two-site cluster model, a local current operator can be defined in the following form:

$$\hat{j} = i \sum_X (\hat{d}_A^Y (\hat{d}_B - \hat{d}_A) - (\hat{d}_B^Y - \hat{d}_A^Y) \hat{d}_A)$$

where the direction of current is that of intra-cluster hopping. This is basically a lattice version of current operator which takes a more familiar differential form in a continuum limit. Then, the Kubo formula for the paramagnetic part of optical conductivity $\chi_{jj}^{para}(\omega)$ is given in terms of the following retarded current-current correlation function $\chi_{jj}(\omega)$:

$$\chi_{jj}(\omega) = i \int_0^{\infty} dt e^{i\omega t} \langle [\hat{j}(t); \hat{j}(0)] \rangle$$

$$\chi_{jj}^{para}(\omega) = i \frac{\chi_{jj}(\omega)}{\omega}$$

Since our clusters only have two sites, only the longitudinal part can be defined. As in the case of spin dynamics, we first calculate the following imaginary-time causal current-current correlation function:

$$\chi_{jj}(\omega) = \langle \hat{j}(\omega) \hat{j}(\omega) \rangle$$

$$= \frac{\text{Tr}_{\text{local}} \hat{D} \hat{D}^Y \hat{j}(\omega) \hat{j}(\omega) e^{S_{eff}}}{Z_{MF}}$$

The detailed form of $X_{jj}(\omega)$ is omitted here [8]. Then, $\chi''_{jj}(\omega)$ can be obtained by the fluctuation-dissipation theorem and analytic continuation:

$$\chi''_{jj}(\omega) = \frac{1}{i} \frac{e^{-\beta\hbar\omega}}{1 - e^{-\beta\hbar\omega}} X_{jj}(\omega)$$

We plot $\text{Re}[\chi''_{jj}(\omega)]$ for $x = 0.3$ and $x = 0.7$ in Fig.11. For $x = 0.7$ (Fig.11 (a)), at higher temperatures, a Druide-like peak is visible due to the fact that the single-particle spectrum has a nonzero weight at E_F (Please see Fig.4 (a)). As the temperature is lowered, the Druide-like weight diminishes and eventually a gap opens up as superconductivity develops. Even when the system passes into the superconducting phase, since the single particle spectrum does not become fully gapped, a small weight still remains in the low energy sectors above $T = 16$. Again, this is due to fluctuation effects which are not included in the BCS theory. The size of the gap is quantitatively consistent with a single-particle gap (i.e., $\omega_{\text{optical}} \approx 2 \omega_{\text{1particle}}$). At this doping, a charge gap feature (i.e., transition between the lower and upper Hubbard bands as seen in Fig.11 (a)) is visible for all temperatures. A feature corresponding to the quasiparticle peaks in the SC state becomes visible as the temperature is lowered ($T = 24$). In Fig.11 (b) (for $x = 0.3$), a large Druide-like peak appears at high temperatures due to a substantial weight at E_F in the single-particle spectrum (Fig.4 (b)). As the temperature decreases, the weight in the low energy sectors disappears and a gap feature develops. Similarly, due to residual single-particle weight at E_F , a robust gap does not develop in charge spectra until the temperature is lowered to $T = 24$. Please note that a feature for the charge gap for $x = 0.3$ is hardly visible, which is consistent with our single-particle spectra at this doping (Fig.4 (b)). This is basically due to a low electron density. An additional feature on the quasiparticle peak (i.e., the feature at the gap edge), however, is much more robust at $x = 0.3$ (as can be expected from Fig.4 (b)) and starts to show up already at $T = 16$. This feature on the gap edge has been observed in the infrared spectra for the optimally doped both single and bi-layer high- T_c materials. The size of the gap for $x = 0.3$ is reduced from that for $x = 0.7$ and is also quantitatively consistent with the single-particle gap as shown in Fig.4 (b). Please note the wide range of energy scales over which the weight is redistributed as a function of temperature. This strongly temperature-dependent spectral weight has been observed in the optical conductivity spectrum of high- T_c cuprates [44] and suggests that the charges participating in the pairing are strongly correlated.

What we showed (numerically) in the above is basically that a paramagnetic current disappears in the superconducting phase below a certain energy scale (optical). Therefore, this will naturally lead to the onset of the Meissner effect caused by a residual diamagnetic response which comes from the mobile Cooper pairs. The magnitude of the diamagnetic response is proportional to the Cooper pair density.

3. Pair degrees of freedom We now turn to the particle-particle channel. The quantity of interest is the pair-pair correlation function. This function basically contains information on the amplitude fluctuations of the superconducting order parameter. A local d-wave like pair-pair correlation function $\chi_d(\mathbf{l})$ can be defined in the following way:

$$\chi_d(\mathbf{l}) = \int_{-1}^1 dt e^{i\mathbf{l}\cdot\mathbf{t}} \langle \hat{\chi}_d^x(\mathbf{t}) \hat{\chi}_d^y(0) \rangle$$

where a local d-wave order parameter centered at a particular A-site is defined as:

$$\begin{aligned} \hat{\chi}_d^y(\mathbf{A}; \mathbf{t}) = & \hat{c}_{A''}^y(\mathbf{t}) \hat{c}_{B_{1\#}}^y(\mathbf{t}) + \hat{c}_{A''}^y(\mathbf{t}) \hat{c}_{B_{2\#}}^y(\mathbf{t}) \\ & \hat{c}_{A''}^y(\mathbf{t}) \hat{c}_{B_{3\#}}^y(\mathbf{t}) - \hat{c}_{A''}^y(\mathbf{t}) \hat{c}_{B_{4\#}}^y(\mathbf{t}) \\ & \hat{c}_{A_{\#}}^y(\mathbf{t}) \hat{c}_{B_{1''}}^y(\mathbf{t}) - \hat{c}_{A_{\#}}^y(\mathbf{t}) \hat{c}_{B_{2''}}^y(\mathbf{t}) \\ & + \hat{c}_{A_{\#}}^y(\mathbf{t}) \hat{c}_{B_{3''}}^y(\mathbf{t}) + \hat{c}_{A_{\#}}^y(\mathbf{t}) \hat{c}_{B_{4''}}^y(\mathbf{t}) \end{aligned}$$

Please note that each pairing for a given nearest-neighbours appears as a singlet which is a direct consequence of taking a zero center-of-mass momentum of the pair (please see below). This expression can be obtained by simply transforming back to real space the following more familiar definition of d-wave operator in 2d momentum space:

$$\hat{\chi}_d^y(\mathbf{t}) = \sum_{\mathbf{p}=(p_x, p_y)}^X (\cos(p_x) - \cos(p_y)) \hat{c}_{\mathbf{p}''}^y(\mathbf{t}) \hat{c}_{\mathbf{p}\#}^y(\mathbf{t})$$

After performing an inverse Fourier transformation, this leads to the following (global) d-wave like operator which is basically a sum of the above local d-wave operator over the all A-sites:

$$\hat{y}_d(t) = \sum_A \hat{y}_d(A;t)$$

The choice of A-site as a reference is arbitrary and B-sites could be chosen just as well.

Since the clusters only have two sites, we need to make an assumption about the symmetry of the dynamics, namely a rotational symmetry among the four nearest-neighborhoods. The above $\hat{y}_d(!)$ is defined with respect to a particular A-site and contains the pairing correlation between its four nearest-neighbor B-sites. Here, we basically make the assumption that the dynamics of these four pairings are the same except for their phases. We view this as a way to represent the effects of inter-cluster correlations within the constraints of our model[13]. Therefore, the above local $\hat{y}_d(A;!)$ can be collapsed into a single two-site cluster. Then, we calculate its corresponding imaginary-time causal correlation function:

$$\begin{aligned} \langle \hat{y}_d(\tau) \hat{y}_d(0) \rangle &= \langle \hat{y}_d(\tau) \hat{y}_d(0) \rangle \\ &= 4 \langle F_{AB}^{\#\#(1)}(\tau; 0) E_{BA}^{\#\#(1)}(0; 0) \rangle \quad (1) \\ &+ 4 \langle F_{BA}^{\#\#(1)}(\tau; 0) E_{AB}^{\#\#(1)}(0; 0) \rangle \quad (1) \\ &+ 4 \langle F_{AB}^{\#\#(1)}(\tau; 0) E_{AB}^{\#\#(1)}(0; 0) \rangle \quad (1) \\ &+ 4 \langle F_{BA}^{\#\#(1)}(\tau; 0) E_{BA}^{\#\#(1)}(0; 0) \rangle \quad (1) \\ &4 \langle G_{AB}^{\#\#\#(1)}(\tau; 0) G_{AB}^{\#\#\#(1)}(0; 0) \rangle \quad (1) \\ &4 \langle G_{BA}^{\#\#\#(1)}(\tau; 0) G_{BA}^{\#\#\#(1)}(0; 0) \rangle \quad (1) \\ &\langle G_{AA}^{\#\#\#(1)}(\tau; 0) G_{BB}^{\#\#\#(1)}(0; 0) \rangle \quad (1) \\ &\langle G_{BB}^{\#\#\#(1)}(\tau; 0) G_{AA}^{\#\#\#(1)}(0; 0) \rangle \quad (1) \\ &+ \langle G_{AA}^{\#\#\#(1)}(\tau; 0) + G_{BB}^{\#\#\#(1)}(\tau; 0) \rangle \quad (1) \end{aligned} \quad (10)$$

where $\langle \hat{y}_d(\tau) \hat{y}_d(0) \rangle$ is an average per pair. Basically, the product of F's and G's correspond to a (local) pair hopping and pair breaking fluctuations, respectively. After

the analytic continuation (Maximum Entropy), we finally obtain a local dynamical pair-pair correlation function $\chi_d(\omega)$.

We plot $\chi_d(\omega)$ for $x = 0.7$ (Fig.12 (a)) and $x = 0.3$ (Fig.12 (b)). We see that for both dopings, as the temperature is lowered, a narrow feature grows around $\omega = 0$ which indicates that the superconducting order parameter develops a well-defined static component. The temperature at which this narrow feature develops basically corresponds to T_c determined from the onset of instantaneous nearest-neighbor pairing correlation.

From a phenomenological point of view, pair hopping and pair breaking fluctuations correspond to short-wavelength phase and amplitude fluctuation of the superconducting order parameter, respectively. The latter is more intuitively transparent but the former becomes readily clear if one notes that:

$$\begin{aligned} \text{(pair hopping)} \quad t_{\text{pair}} &= \sum_{i,j} (\hat{c}_{d;i}^\dagger \hat{c}_{d;j} + \hat{c}_{d;j}^\dagger \hat{c}_{d;i}) \\ &= t_{\text{pair sc}} \cos(\phi_i - \phi_j) \end{aligned}$$

where

$$\langle \hat{c}_{d;i}^\dagger \rangle = \langle \hat{c}_{d;i} \rangle = \frac{p_{\text{sc}}}{e^{i\phi_i}} \quad (11)$$

Therefore, we can see in more detail the nature of the onset of a superconducting phase by studying both pair hopping ($F \leftrightarrow F$ terms in (15)) and pair breaking ($G \leftrightarrow G$ terms in (15)) fluctuations. From detailed studies [45], we found that pair breaking fluctuations are more strongly gapped at T_c for $x = 0.7$ than for $x = 0.3$, and this implies that the amplitude fluctuations are more enhanced for $x = 0.3$ when superconductivity switches on. These findings basically suggest that Cooper pairs are more tightly bound in the low doping region (which is consistent with the doping evolution of the single-particle gap). Since phase fluctuations are typically energetically cheaper than amplitude fluctuations (this will typically be a gapless Goldstone mode in the long wavelength limit), a remedy for the over-estimate of T_c in the low doping region may be sought by incorporating a phase fluctuation mechanism, or equivalently charge localization in the dual picture. (In the present model, the coherent pair-hopping fluctuations are gapless as seen in Fig.12, and phase coherence can not be suppressed, i.e., a charge localization mechanism is absent.) Although such

localization mechanisms have been proposed [46, 47], phenomenology in the lightly doped region is still under debate [48]. Please note that the physics which governs global phase coherence is a low energy long-wavelength phenomenon (depending on the localization length of Cooper pairs) and is thus not possible to address by the present approach based on the small cluster size.

D. Equilibrium properties and phase diagram

Since our main focus is antiferromagnetism and superconductivity, we investigate those two phases. We show our results both with and without the inter-cluster coupling.

An antiferromagnetic phase is signaled by the onset of the thermal average of a staggered magnetization induced by an infinitesimal staggered field. Here, instead, we chose to induce symmetry breaking by appropriately initializing the Ising variables for each sublattice. Although the staggered magnetization is in principle a vector order parameter a natural choice is its z-component, since the Hubbard-Stratonovich decomposition was performed along the z-axis. This is given as:

$$\begin{aligned}
 \langle \hat{M}^z \rangle &= \langle \hat{S}_A^z \rangle - \langle \hat{S}_B^z \rangle \\
 \langle \hat{S}_A^z \rangle &= \langle \hat{n}_A^\uparrow \rangle - \langle \hat{n}_A^\downarrow \rangle \\
 \langle \hat{S}_B^z \rangle &= \langle \hat{n}_B^\uparrow \rangle - \langle \hat{n}_B^\downarrow \rangle
 \end{aligned}$$

where $\langle \dots \rangle$ means a thermal average. In Fig.13 (a), the staggered magnetization, $\langle \hat{M}^z \rangle$, is plotted at half-filling as a function of temperature. Since superconductivity does not set in exactly at half-filling, there is no distinction between the two cases. The staggered magnetization disappears roughly at $T = 6$. Upon doping, $\langle \hat{M}^z \rangle$ almost suddenly drops and disappears before T reaches 0.009. A detailed study of the destruction of antiferromagnetism as a function of doping is outside the scope of this paper, and we did not sample sufficiently many doping levels to determine the nature of transition, such as the order of transition.

Similarly, if we employ the definition of the BCS picture, an onset of superconductivity can be defined as the onset of an average of equal-time anomalous Green's

function:

$$\mathcal{F}(0)^2 = \mathcal{F}_{AB}^{\#\#}(0)^2 + \mathcal{F}_{BA}^{\#\#}(0)^2 + \mathcal{F}_{AB}^{\#\#}(0)^2 + \mathcal{F}_{BA}^{\#\#}(0)^2$$

All the on-site pairing components, $F_{AA}^{\#\#}(0)$, $F_{AA}^{\#\#}(0)$, $F_{BB}^{\#\#}(0)$ and $F_{BB}^{\#\#}(0)$, are always one to three orders of magnitude smaller. We turn on a small ℓ and see if the system can sustain a finite $\mathcal{F}(0)^2$. Therefore, according to linear response theory, the appearance of a finite $\mathcal{F}(0)^2$ basically corresponds to divergence of the pairing fluctuations. In Fig.13, $\mathcal{F}(0)^2$ is also plotted as a function of doping for $\ell = 16$ (Fig.13 (b)) and as a function of temperature for large doping (Fig.13 (c)) and small doping (Fig.13 (d)). We found that the inclusion of inter-cluster coupling systematically enhances T_c [8]. The doping which gives a maximum $\mathcal{F}(0)^2$ seems to be somewhere between $x = 0.4$ ($\ell = 0.13$) and $x = 0.3$ ($\ell = 0.17$) for both cases. A determination of the doping which gives a maximum T_c requires a detailed study involving varying both temperature and doping and was difficult to identify with the same accuracy (it appears to be located at least between $x = 0.09$ and $x = 0.17$). Note that a superconducting phase appears as soon as the system is doped.

In Fig.14, we show the phase diagram as a function of doping and temperature in the presence of inter-cluster coupling. (A phase diagram without inter-cluster pairing is also shown here. The overall topography is quite similar [8].) Note that the overall topography is quite consistent with that of high- T_c cuprates: a sudden suppression of AF order away from half-filling, an upper critical doping for superconductivity at roughly $x_c = 0.3$ and an optimal doping is located $0.13 < x < 0.17$. For $\ell = 0.1$, all the qualitative features are essentially the same although the upper critical doping and the staggered magnetization at half-filling appear to increase slightly.

One notices, however, that a superconducting amplitude is quite alive even in a lightly doped region, i.e., the lower critical doping is essentially zero. This feature was found for a related model in a BCS mean-field approximation [14] (which can be thought of as a static version of the present approach) and later interpreted as the onset of a phase stiffness (i.e., the amplitude part) of the superconducting order parameter [46] which exactly corresponds to $\mathcal{F}(0)^2$ here. A locally constructed superconductivity was also found to coexist with antiferromagnetism for a relatively wide range of doping in the dynamical mean-field theory study of equilibrium state of a cluster model in which local dynamics are more constrained [13]. As mentioned in the previous section, the physics of underdoped region is still under debate.

IV . Sum m ary and C onclusions.

As m entioned previously, the relatively short coherence and spin-spin correlation lengths which are observed in the in high- T_c cuprates constitute the key motivation of the present study as well as underpinning the basis of our approach. The subject of this paper is to investigate the role of short-range quantum fluctuations in high- T_c superconductivity and, in particular, the interplay between pairing and spin fluctuations. In order to achieve a more complete understanding of the strongly coupled dynamics whose calculation goes beyond the bounds of BCS mean-field we apply dynamical mean-field theory to a simple 2-atom cluster model. We showed that this model, despite its simplicity, not only reproduces the main characteristic features of high- T_c cuprates (i.e., the basic topography of the phase diagram, a quasiparticle feature in single-particle spectra, the spin-gap, neutron resonance, d-wave-like pairing, etc) with qualitative and semi-quantitative consistency, but also revealed a strong correlation between coherent short-ranged antiferromagnetic spin fluctuations and pairing correlations: i.e., if superconductivity is suppressed the antiferromagnetic spin fluctuations lose their coherence. Thus our approach allows us to directly study the relation between the dynamics of the spin and pair degrees of freedom.

We would like to emphasize that the present model was constructed from strongly correlated electron degrees of freedom only and no prior assumption was made for the existence of any intermediate energy scale which typically represents some sort of composite bosonic degrees of freedom in either particle-hole or particle-particle channel. In the present formalism, bosonic degrees of freedom arise naturally as a consequence of gap formation in the single-particle sector. In our model, away from half filling, coherence builds up in a singlet particle-particle channel and this is accompanied by a development of coherence in the staggered spin channel at some characteristic energy scale. The only nontrivial assumption that we put into the present model is basically that the correlation length of spin and pairing fluctuations is sufficiently short and that antiferromagnetic fluctuations are a relevant spin fluctuation mode to consider. In this context we have been able to show that the spin fluctuation resonance which

has been discussed by a number of authors [17, 18] as a spin - ip exciton-like mode is a generic feature of our model. This suggests that it survives beyond the RPA approach and should not depend on details of the band structure of the system . Thus it appears to be an intrinsic property of the strongly coupled superconducting state in the presence of strong on-site repulsion .

From our results on the single particle excitations of the model, and the fact that we can correlate the "hump feature" seen in ARPES spectra with that seen in our model, we conclude that the spectral weight of the spin fluctuation resonance is sufficient to show up as an energy loss peak in the photoemission spectra. This is in contrast to recent arguments [34, 33] suggesting that details of the band structure are important in this interpretation of the ARPES data. From the point of view of the local physics represented in our model, it appears that this feature is an intrinsic property of Hubbard-type models of superconductivity.

The present approach is essentially an analogue of Weiss mean-field theory in which fluctuations along the imaginary time are exactly treated but all the spatial fluctuations whose wavelengths are longer than the size of the cluster are averaged out. Unlike theories which are based on momentum space representation, it is based on a local picture. Therefore, when the physics in the thermodynamic limit is dominated by low-lying long-wavelength modes, this local description is expected to break down. (When the correlation length becomes sufficiently longer than the cluster size but still finite, the present model will incorrectly assume that true long-range order is established). Typically, it is the dimensionality of the system which plays a crucial role in deciding the fate of the thermodynamic limit when long-wavelength fluctuations dominate. (Of course, the length scale of interactions among the local order parameters, short-ranged or long-ranged, is also important and this is assumed to be of short-range in the present study). Therefore, physics which depends on the dimensionality in an essential way will be difficult to address in this approach. (This approach is essentially a $d+1$ dimensional formalism.) Instead, the present model is looking at the portion of physics which is rather insensitive to the dimensionality, i.e. the short-range short-wavelength modes. Such features are relatively dimension independent (indeed, superconductivity and similar anomalous features have been reported in quasi-1D doped Hubbard ladder systems as well [49]).

Before we conclude, we note that recent studies [13, 16] have looked at dynamical properties of four-site cluster models. Although these authors have not yet investigated the excitation spectra of such models, we expect them to lead to qualitatively the same conclusions that we have reached based on our 2-site cluster model. A four-site square cluster model would also allow consideration of other kinds of long range order such as a chiral flux phase [50, 51]. A four-site cluster model would also allow for study of the dynamics of ϕ -operators in the presence of broken symmetry phases (effectively in a thermodynamic limit) and the connection between $SO(5)$ symmetry [52, 53] and superconductivity. This would be complementary to results of exact numerical work [54] for finite clusters.

The present approach is to transform the original lattice problem to an effective self-consistent local which can be exactly solved in principle. Thus, it can provide essentially exact solutions to the original problem within the range of validity of this transformation. Certain aspects of high- T_c superconductivity appear to fit reasonably well into the regime in which this transformation is valid. The present model is perhaps the simplest nontrivial one in the context of a self-consistent cluster model in the dynamical mean-field theory approach. Yet, it appears to succeed in addressing some nontrivial aspects of strongly correlated electron systems which would be difficult to approach by other means. The results we have presented clearly suggest that as long as the physics at hand is of short-range this approach can be quite effective and promising.

In summary, we constructed a self-consistent two-site cluster model in the dynamical mean-field limit in which short-range short-wavelength fluctuations of charge and spin degrees of freedom are treated exactly in the presence of superconductivity. The equilibrium properties of our model (superconductivity and antiferromagnetism) as a function of doping and temperature reproduce the overall qualitative and basic quantitative features of the phase diagram of high- T_c cuprates. The behavior of single-particle and two-particle spectra of our model in the superconducting phase can be interpreted to give a consistent account of anomalous features of high- T_c cuprates such as the pseudogap (charge and spin) and resonance observed in ARPES, INS, NMR and other optical measurements.

ACKNOWLEDGEMENTS

We acknowledge the NSF for support through Grant No. DMR 9418964 and through the Center for Materials Research at Stanford University, and the San Diego Super-computer Center for a grant of computer time.

APPENDIX A : Complete self-consistency equation

If we systematically integrate out all the ligand degrees of freedom, we obtain the following self-consistency condition which constitutes the lattice nature of the problem. The physical meaning of each term can be diagrammatically illustrated in the same manner as we showed in sec.III:

$$\begin{aligned}
 G_{AA}'''(i!_n) &= i!_n \quad d + \quad + h_z \quad \frac{U}{2} \quad t^2 G_{BB}'''(i!_n) \\
 &\quad t^2 \begin{matrix} \# \\ AB \end{matrix} \begin{matrix} \# \\ BA \end{matrix} G_{BB}^{##}(i!_n) \\
 &\quad + t^2 (\begin{matrix} \# \\ AB \end{matrix} F_{BB}^{##}(i!_n) + \begin{matrix} \# \\ BA \end{matrix} F_{BB}^{##}(i!_n)) \\
 G_{BB}'''(i!_n) &= i!_n \quad d + \quad h_z \quad \frac{U}{2} \quad t^2 G_{AA}'''(i!_n) \\
 &\quad t^2 \begin{matrix} \# \\ BA \end{matrix} \begin{matrix} \# \\ AB \end{matrix} G_{AA}^{##}(i!_n) \\
 &\quad + t^2 (\begin{matrix} \# \\ BA \end{matrix} F_{AA}^{##}(i!_n) + \begin{matrix} \# \\ AB \end{matrix} F_{AA}^{##}(i!_n)) \\
 G_{AA}^{##}(i!_n) &= i!_n + \quad d \quad + h_z + \frac{U}{2} \quad t^2 G_{BB}^{##}(i!_n) \\
 &\quad t^2 \begin{matrix} \# \\ AB \end{matrix} \begin{matrix} \# \\ BA \end{matrix} G_{BB}'''(i!_n) \\
 &\quad t^2 (\begin{matrix} \# \\ BA \end{matrix} F_{BB}^{##}(i!_n) + \begin{matrix} \# \\ AB \end{matrix} F_{BB}^{##}(i!_n)) \\
 G_{BB}^{##}(i!_n) &= i!_n + \quad d \quad h_z + \frac{U}{2} \quad t^2 G_{AA}^{##}(i!_n) \\
 &\quad t^2 \begin{matrix} \# \\ BA \end{matrix} \begin{matrix} \# \\ AB \end{matrix} G_{AA}'''(i!_n) \\
 &\quad t^2 (\begin{matrix} \# \\ AB \end{matrix} F_{AA}^{##}(i!_n) + \begin{matrix} \# \\ BA \end{matrix} F_{AA}^{##}(i!_n))
 \end{aligned}$$

$$\begin{aligned}
 G_{AB}'''(i!_n) &= t^0 \quad t^2 G_{BA}'''(i!_n) \\
 &\quad t^2 \begin{matrix} \# \\ AB \end{matrix} \begin{matrix} \# \\ AB \end{matrix} G_{BA}^{##}(i!_n) \\
 &\quad + t^2 (\begin{matrix} \# \\ AB \end{matrix} F_{BA}^{##}(i!_n) + \begin{matrix} \# \\ AB \end{matrix} F_{BA}^{##}(i!_n))
 \end{aligned}$$

$$\begin{aligned}
G_{BA}'''(i!_n) &= t^0 t^2 G_{AB}'''(i!_n) \\
&\quad t^2 \begin{matrix} \# \\ BA \end{matrix} \begin{matrix} \# \\ BA \end{matrix} G_{AB}^{##}(i!_n) \\
&\quad + t^2 (\begin{matrix} \# \\ BA \end{matrix} F_{AB}^{\#\#}(i!_n) + \begin{matrix} \# \\ BA \end{matrix} F_{AB}^{\#\#}(i!_n)) \\
G_{AB}^{##}(i!_n) &= t^0 t^2 G_{BA}^{##}(i!_n) \\
&\quad t^2 \begin{matrix} \# \\ AB \end{matrix} \begin{matrix} \# \\ AB \end{matrix} G_{BA}'''(i!_n) \\
&\quad t^2 (\begin{matrix} \# \\ AB \end{matrix} F_{BA}^{\#\#}(i!_n) + \begin{matrix} \# \\ AB \end{matrix} F_{BA}^{\#\#}(i!_n)) \\
G_{BA}^{##}(i!_n) &= t^0 t^2 G_{AB}^{##}(i!_n) \\
&\quad t^2 \begin{matrix} \# \\ BA \end{matrix} \begin{matrix} \# \\ BA \end{matrix} G_{AB}'''(i!_n) \\
&\quad t^2 (\begin{matrix} \# \\ BA \end{matrix} F_{AB}^{\#\#}(i!_n) + \begin{matrix} \# \\ BA \end{matrix} F_{AB}^{\#\#}(i!_n))
\end{aligned}$$

$$\begin{aligned}
F_{AA}^{\#\#}(i!_n) &= t^2 F_{BB}^{\#\#}(i!_n) \\
&\quad t^2 \begin{matrix} \# \\ AB \end{matrix} \begin{matrix} \# \\ BA \end{matrix} F_{BB}^{\#\#}(i!_n) \\
&\quad t^2 (\begin{matrix} \# \\ AB \end{matrix} G_{BB}^{##}(i!_n) \quad \begin{matrix} \# \\ BA \end{matrix} G_{BB}'''(i!_n)) \\
F_{AA}^{\#\#}(i!_n) &= t^2 F_{BB}^{\#\#}(i!_n) \\
&\quad t^2 \begin{matrix} \# \\ BA \end{matrix} \begin{matrix} \# \\ AB \end{matrix} F_{BB}^{\#\#}(i!_n) \\
&\quad t^2 (\begin{matrix} \# \\ BA \end{matrix} G_{BB}^{##}(i!_n) \quad \begin{matrix} \# \\ AB \end{matrix} G_{BB}'''(i!_n)) \\
F_{BB}^{\#\#}(i!_n) &= t^2 F_{AA}^{\#\#}(i!_n) \\
&\quad t^2 \begin{matrix} \# \\ AB \end{matrix} \begin{matrix} \# \\ BA \end{matrix} F_{AA}^{\#\#}(i!_n) \\
&\quad t^2 (\begin{matrix} \# \\ BA \end{matrix} G_{AA}^{##}(i!_n) \quad \begin{matrix} \# \\ AB \end{matrix} G_{AA}'''(i!_n)) \\
F_{BB}^{\#\#}(i!_n) &= t^2 F_{AA}^{\#\#}(i!_n) \\
&\quad t^2 \begin{matrix} \# \\ AB \end{matrix} \begin{matrix} \# \\ BA \end{matrix} F_{AA}^{\#\#}(i!_n) \\
&\quad t^2 (\begin{matrix} \# \\ AB \end{matrix} G_{AA}^{##}(i!_n) \quad \begin{matrix} \# \\ BA \end{matrix} G_{AA}'''(i!_n))
\end{aligned}$$

$$\begin{aligned}
F_{AB}^{\#\#}(i!_n) &= \quad + t^2 F_{BA}^{\#\#}(i!_n) \\
&\quad t^2 (\begin{matrix} \# \\ AB \end{matrix})^2 F_{BA}^{\#\#}(i!_n) \\
&\quad t^2 \begin{matrix} \# \\ AB \end{matrix} (G_{BA}^{##}(i!_n) \quad G_{BA}'''(i!_n)) \\
F_{BA}^{\#\#}(i!_n) &= \quad + t^2 F_{AB}^{\#\#}(i!_n) \\
&\quad t^2 (\begin{matrix} \# \\ BA \end{matrix})^2 F_{AB}^{\#\#}(i!_n) \\
&\quad t^2 \begin{matrix} \# \\ BA \end{matrix} (G_{AB}^{##}(i!_n) \quad G_{AB}'''(i!_n))
\end{aligned}$$

$$\begin{aligned}
F_{BA}^{\#\#}(\mathbf{i}!_n) &= \quad + \mathcal{E}^2 F_{AB}^{\#\#}(\mathbf{i}!_n) \\
&\quad \mathcal{E}^2 ({}^{\#\#}_{BA})^2 F_{AB}^{\#\#}(\mathbf{i}!_n) \\
&\quad \mathcal{E}^2 {}^{\#\#}_{BA} (G_{AB}^{\#\#}(\mathbf{i}!_n) \quad G_{AB}^{\#\#\#}(\mathbf{i}!_n)) \\
F_{AB}^{\#\#}(\mathbf{i}!_n) &= \quad + \mathcal{E}^2 F_{BA}^{\#\#}(\mathbf{i}!_n) \\
&\quad \mathcal{E}^2 ({}^{\#\#}_{AB})^2 F_{BA}^{\#\#}(\mathbf{i}!_n) \\
&\quad \mathcal{E}^2 {}^{\#\#}_{AB} (G_{BA}^{\#\#}(\mathbf{i}!_n) \quad G_{BA}^{\#\#\#}(\mathbf{i}!_n))
\end{aligned}$$

APPENDIX B : Manifestation of a sublattice symmetry in the formula of the accept ratio

Since the Nambu-Gorkov representation is used in (9), we first need to transform to the usual representation. This can be done by transforming only the down spin components in the following way:

$$\begin{aligned}
G_{AA}^{\#\#}(\mathbf{i}; \mathbf{i}) &\rightarrow 1 \quad G_{AA}^{\#\#}(\mathbf{i}; \mathbf{i}) \\
G_{BB}^{\#\#}(\mathbf{i}; \mathbf{i}) &\rightarrow 1 \quad G_{BB}^{\#\#}(\mathbf{i}; \mathbf{i})
\end{aligned}$$

This will transform the accept ratio to the following form :

$$\begin{aligned}
R_A(\mathbf{i}) &= ((e^{A(\mathbf{i})} \quad e^{-A(\mathbf{i})}) G_{AA}^{\#\#\#}(\mathbf{i}; \mathbf{i}) + e^{A(\mathbf{i})} \\
&\quad (e^{-A(\mathbf{i})} \quad e^{A(\mathbf{i})}) G_{AA}^{\#\#}(\mathbf{i}; \mathbf{i}) + e^{A(\mathbf{i})} \\
&\quad (e^{A(\mathbf{i})} \quad e^{-A(\mathbf{i})})^2 F_{AA}^{\#\#}(\mathbf{i}; \mathbf{i}) F_{AA}^{\#\#}(\mathbf{i}; \mathbf{i})) \\
R_B(\mathbf{i}) &= ((e^{B(\mathbf{i})} \quad e^{-B(\mathbf{i})}) G_{BB}^{\#\#\#}(\mathbf{i}; \mathbf{i}) + e^{B(\mathbf{i})} \\
&\quad (e^{-B(\mathbf{i})} \quad e^{B(\mathbf{i})}) G_{BB}^{\#\#}(\mathbf{i}; \mathbf{i}) + e^{B(\mathbf{i})} \\
&\quad (e^{B(\mathbf{i})} \quad e^{-B(\mathbf{i})})^2 F_{BB}^{\#\#}(\mathbf{i}; \mathbf{i}) F_{BB}^{\#\#}(\mathbf{i}; \mathbf{i}))
\end{aligned}$$

in which the sublattice symmetry is manifestly apparent.

APPENDIX C : Calculation of $\chi^z(\mathbf{Q})$

In this appendix, we show the details of the procedure to compute a staggered spin susceptibility $\chi^z(\mathbf{Q})$ from an imaginary-time causal staggered spin-spin correlation function which is given as:

$$S_z(\mathbf{Q}; \omega) = \frac{\langle \hat{M}_z(\mathbf{Q}) \hat{M}_z(\mathbf{Q})^\dagger \rangle}{Z_{MF}}$$

The above trace involves four point correlators and a Wick contraction needs to be performed. Since the effective action is bilinearized by the Hubbard-Stratonovich transformation, the functional integral over the fermionic degrees of freedom can be exactly performed and the above trace simply becomes a sum of the products of local Green's functions averaged over the Ising variable. In other words, all the vertex corrections at the local level are decoupled by means of Hubbard-Stratonovich transformation and re-absorbed into the dependencies of the local propagators on the Ising variable. For example, the term $\langle \hat{n}_{A\#}(\mathbf{r}) \hat{n}_{B\#}(\mathbf{r}') \rangle$ can be integrated in the following way:

$$\begin{aligned} \langle \hat{n}_{A\#}(\mathbf{r}) \hat{n}_{B\#}(\mathbf{r}') \rangle &= \langle \hat{d}_{A\#}^\dagger(\mathbf{r}) \hat{d}_{A\#}(\mathbf{r}) \hat{d}_{B\#}^\dagger(\mathbf{r}') \hat{d}_{B\#}(\mathbf{r}') \rangle \\ &= \langle G_{AA}^{##(1)}(\mathbf{r}; \mathbf{r}') G_{BB}^{##(1)}(\mathbf{r}') \rangle_{(1)} \\ &\quad \langle G_{AB}^{##(1)}(\mathbf{r}; \mathbf{r}') G_{BA}^{##(1)}(\mathbf{r}') \rangle_{(1)} \end{aligned}$$

where $\langle \dots \rangle_{(1)}$ means an averaging over the Ising variable. The normal order for down spin components is reversed due to the Nambu representation. The full expression of $S_z(\mathbf{Q}; \omega)$ becomes quite lengthy and is omitted here [8]. The averaging over the Ising variable is performed by the QMC sampling. Since $S_z(\mathbf{Q}; \omega)$ is a scattering function (i.e., fluctuation of a spin degrees of freedom), the transfer function which defines the relation between the imaginary-time and real-time quantities becomes:

$$S_z(\mathcal{Q}; \beta) = \frac{1}{2} \sum_{\mathcal{Q}} e^{-\beta S_z(\mathcal{Q}; \beta)}$$

where $S_z(\mathcal{Q}; \beta)$ must satisfy the equation of detailed balance $S_z(\mathcal{Q}; \beta) = e^{-\beta} S_z(\mathcal{Q}; \beta)$. (Please note the difference from the fermion operators (10).) Here, the equation of detailed balance can be used as a constraint for the default model in Maximum Entropy [55] or simply absorb it into the transfer function, which is the approach we adopted here.

References

- [1] P. W. Anderson, *Science* 235, 1196 (1987)
- [2] P. Bourges et al., *Physica B* 215, 30 (1995)
- [3] P. Bourges et al., *Phys. Rev. B* 53, 876 (1996)
- [4] P. Bourges et al., *Europhysics Lett.* 38, 313 (1997)
- [5] P. Dai et al., *Phys. Rev. Lett.* 77, 5425 (1996)
- [6] H. F. Fong et al., *Nature* 398, 588 (1999).
- [7] E. W. Hudson et al., *Nature* 411, 920 (2001)
- [8] H. Watanabe, Ph.D. thesis, Stanford University 1999 (unpublished)
- [9] A. Georges and G. Kotliar, *Phys. Rev. B* 45, 6479 (1992)
- [10] W. Metzner and D. Vollhardt, *Phys. Rev. Lett.* 62, 324 (1989)
- [11] A. Georges, G. Kotliar, W. Krauth and M. J. Rozenberg, *Rev. Mod. Phys.* 68, 13 (1996)

- [12] A. Georges, G. Kotliar and W. Krauth, *Z. Phys. B* 92, 313 (1993)
- [13] A. J. Lichtenstein and M. J. Katsnelson *Phys. Rev. B* 62, R 9283 (1999)
- [14] M. Inui, S. Doniach, P. J. Hirschfeld and A. E. Ruckenstein, *Phys. Rev. B* 37, 2320 (1988)
- [15] P. Dickinson and S. Doniach, *Phys Rev B* . 47, 11447 (1993)
- [16] Th. Maier, M. Jarrell, Th. Puschke and J. Keller, *cond-mat/0002352* (2000)
- [17] A. R. Abanov, A. Chubukov and J. Schmalian *Phys. Rev. B* 63, R 0510 (2000).
- [18] J. Brinckmann and P. A. Lee *Phys. Rev. Letts* 82, 2915 (1999).
- [19] M. J. Rozenberg et al., *Phys. Rev. B* 49, 10181 (1994)
- [20] M. Jarrel, *Phys. Rev. Lett.* 69, 169 (1992)
- [21] T. Puschke et al., *Phys. Rev. B* 47, 3553 (1993)
- [22] See, for example, G. Kotliar in *STRONGLY CORRELATED ELECTRON MATERIALS, THE LOS ALAMOS SYMPOSIUM*, (Addison Wesley, 1993)
- [23] A. Schiller and K. Ingersent, *Phys. Rev. Lett.* 75, 113 (1995)
- [24] A. Georges and G. Kotliar, unpublished
- [25] J. E. Hirsch and R. M. Fye, *Phys. Rev. Lett.* 56, 2521 (1986)
- [26] H. Watanabe and S. Doniach, *Phys. Rev. B* 57, 3829 (1998)
- [27] A metal-insulator transition in the presence of antiferromagnetic order where carrier doping is not involved has been analyzed based on the two-band Hubbard model in DMFT [26, 8].
- [28] J. E. Gubematis et al., *Phys. Rev. B* 44, 6011 (1991)
- [29] R. N. Silver, D. S. Sivia and J. E. Gubematis, *Phys. Rev. B* 41, 2380 (1990)
- [30] J. E. Hirsch, *Phys. Rev. B* 28, 4059 (1983)
- [31] J. R. Schrieffer in *Theory of Superconductivity*, (Addison Wesley, 1988)
- [32] P. J. White et al., *Phys. Rev. B* 54, R 15669 (1996)

- [33] A. Abanov, A. V. Chubukov, E. Eschrig, M. R. Norman and J. Schmalian. cond-mat/0112126 (2001)
- [34] H.-Y. Kee, S. A. Kivelson and G. Aeppli cond-mat/0110478 (2001)
- [35] J. M. Harris et al., Phys. Rev. B 54, R15665 (1996)
- [36] H. Ding et al., Phys. Rev. B 54, R9678 (1996)
- [37] J. Rossat-Mignod et al., Physica B 169, 58 (1991)
- [38] J. Rossat-Mignod et al., Physica C 185, 86 (1991)
- [39] J. Rossat-Mignod et al., Physica B 180, 383 (1992)
- [40] H. A. Mook et al., Phys. Rev. Lett. 70, 149 (1993)
- [41] H. F. Fong et al., Phys. Rev. Lett. 78, 713 (1997)
- [42] H. F. Fong et al., Phys. Rev. B 54, 6708 (1996)
- [43] P. Bourges, Phys. Rev. Lett. 80, 1793 (1998)
- [44] T. Startsev et al., Phys. Rev. B 59, 7184 (1999)
- [45] We found that for $\nu = 0.7$, when a narrow peak at $\omega = 0$ in the pair hopping channel (the weight of this peak basically corresponds to the Meissner weight) starts to develop (below $\nu = 10$), the pair breaking channel is roughly gapped $\nu_{\text{particle}} \frac{k_B T}{t} (= \frac{1}{t} \approx 0.2)$ and thus suppressed. On the other hand, for $\nu = 0.3$ when weight starts to develop at $\omega = 0$ in the pair-hopping channel, the pair breaking channel still has significant weight in the low energy sector $\frac{k_B T}{t}$, which implies that the amplitude fluctuations are significantly enhanced for $\nu = 0.3$ near T_c . Since the energy scale for pair breaking exactly matches to the single-particle gap (Fig.4), the distinction between $\nu = 0.7$ and $\nu = 0.3$ essentially comes from a difference in the robustness of a single-particle gap [8].
- [46] S. Doniach and M. Inui, Phys. Rev. B 41, 6668 (1990)
- [47] V. Emery and S. Kivelson, Nature 374, 434 (1995)
- [48] K. Voelker and S. Chakravarty, Phys. Rev. B 64, 235125 (2001)
- [49] M. Uehara et al., J. Phys. Soc. Jpn. 65, 2764 (1996)

- [50] I.K. Aleck and J.B. Marston, *Phys. Rev. B* 37, 3774 (1988)
- [51] X.G. Wen et al, *Phys. Rev. B* 39, 11413 (1989)
- [52] S.C. Zhang, *Science* 275, 1089 (1997)
- [53] E. Denler and S.C. Zhang, *Phys. Rev. Lett.* 75, 4126 (1995)
- [54] W. Hanke et al, *cond-mat/9807015*
- [55] J. D Eisz et al, *Phys. Rev. B* 42, R 4849 (1990)

Figure 1 : A schematic picture of our model. Elliptic curves define the two-site cluster. All sites have the same nonzero U , all inter-cluster hopping have the same t , and all intra-cluster hopping have the same t^0 .

Figure 2 : Evolution of single-particle spectra as a function of temperature without inter-cluster anomalous terms. (a) is for a small doping ($\delta = 0.05$) and (b) for a large doping ($\delta = 0.17$).

Figure 3 : Single-particle spectrum in the normal phase for $\delta = 16$ and $\delta = 0.05$.

Figure 4 : Evolution of single-particle spectra as a function of temperature with inter-cluster anomalous terms. (a) is for small doping ($\delta = 0.04$) and (b) for large doping ($\delta = 0.17$).

Figure 5 : DOS of normal (solid line) and SC (dashed line) state for $\delta = 0.7$ as a function of temperature. A gap feature clearly builds up as the superconducting correlation develops.

Figure 6 : A single-particle gap (diamond), Cooper pair density ($\chi_F(0)^2$, cross) and T_c (square) vs. doping at $\delta = 16$. Vertical units are arbitrary.

Figure 7 : $\chi_z(Q; \omega)$ as a function of temperature for the underdoped region. (a) without inter-cluster pairing and (b) with inter-cluster pairing.

Figure 8 : $\chi_z(Q; \omega)$ as a function of temperature near the optimal doping region. (a) without inter-cluster pairing and (b) with inter-cluster pairing.

Figure 9 : $\chi_z(Q; \omega)$ as a function of doping. (a) without inter-cluster pairing and (b) with inter-cluster pairing.

Figure 10 : $\chi_z(Q; \omega)$ spectra of normal (dash line) and SC (solid line) for $\delta = 16$ and $\delta = 0.3$. Coherence is severely degraded and the gap is filled in the normal phase.

Figure 11 : $\text{Re}[\chi^{\text{para}}(\omega)]$ as a function of temperature for $\delta = 0.7$ (a) and $\delta = 0.3$ (b). The horizontal unit is $2t$ and the vertical unit is arbitrary.

Figure 12 : $\chi_d(\omega)$ as a function of temperature for $\mu = 0.7$ (a) and $\mu = 0.3$ (b). The horizontal unit is $2t$ and the vertical unit is arbitrary.

Figure 13 : (a) M_z vs. temperature at half filling. Units are μ_B and $2t$ for vertical and horizontal axis, respectively. (b) $\chi''(0)$ vs. doping at $\mu = 16$. A unit for the vertical axis is arbitrary. $\chi''(0)$ vs. temperature for $\mu = 0.7$ (c) and $\mu = 0.3$ (d).

Figure 14 : Schematic phase diagram obtained based on our model. The onset of SC was determined by the appearance of a thermal average of an instantaneous pairing amplitude. Error bars correspond to the size of increments of sampling points we studied.

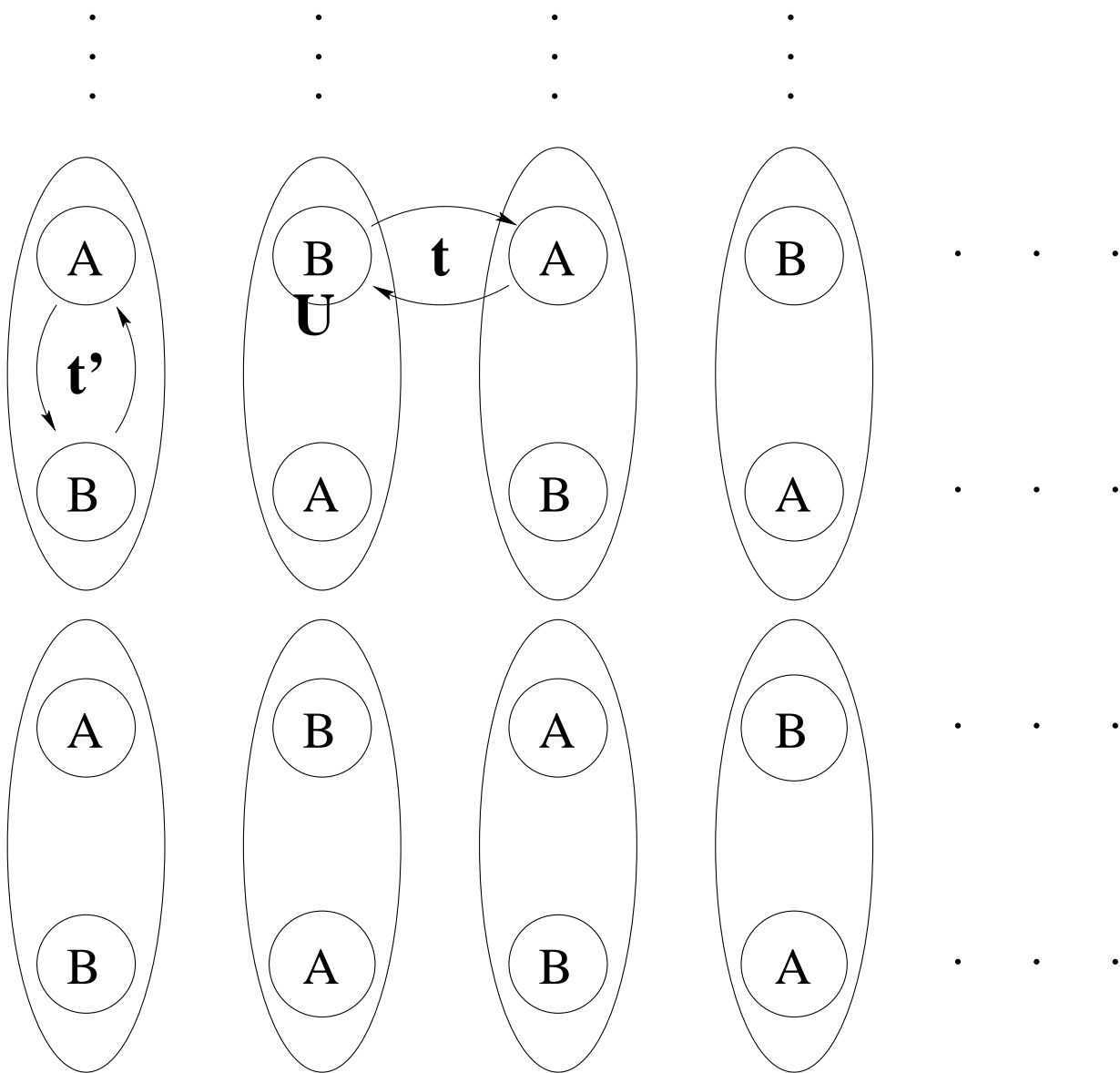


Figure 1 : A schematic picture of our model. Elliptic curves define the two-site cluster. All sites have the same nonzero U , all inter-cluster hopping have the same t , and all intra-cluster hopping have the same t^0 .

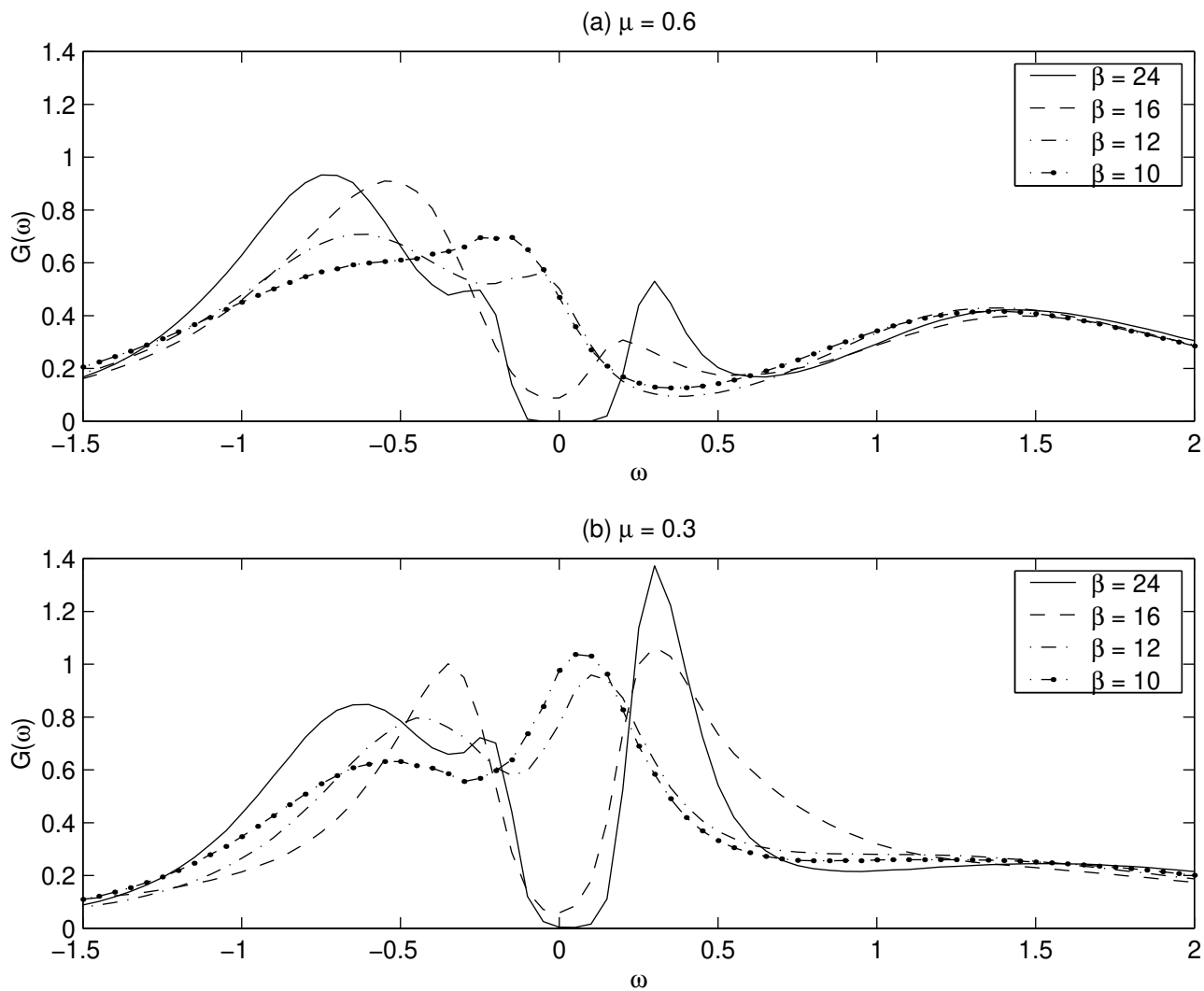


Figure 2 : Evolution of single-particle spectra as a function of temperature without inter-cluster anomalous terms. (a) is for a small doping ($\mu = 0.05$) and (b) for a large doping ($\mu = 0.17$).

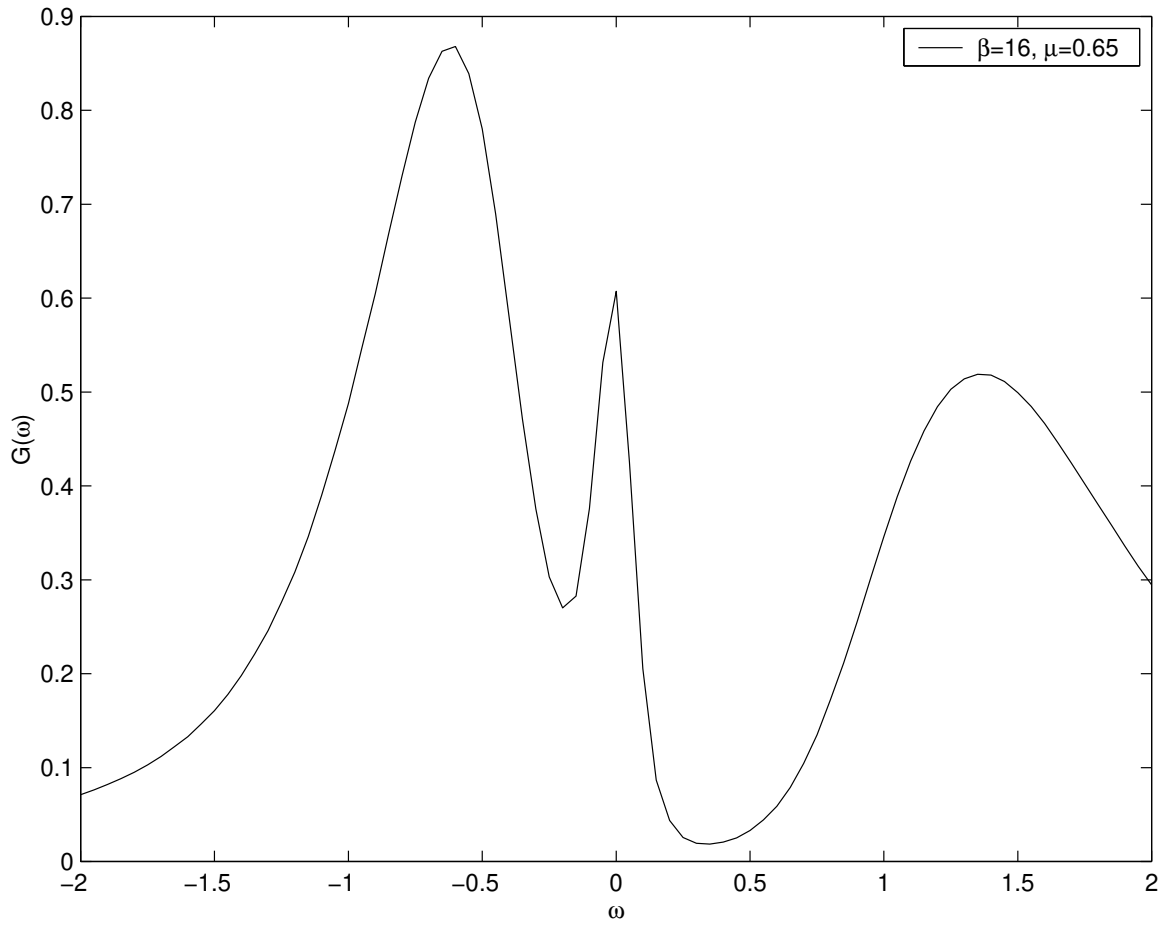


Figure 3 : Single-particle spectrum in the normal phase for $\beta = 16$ and $\mu = 0.65$.

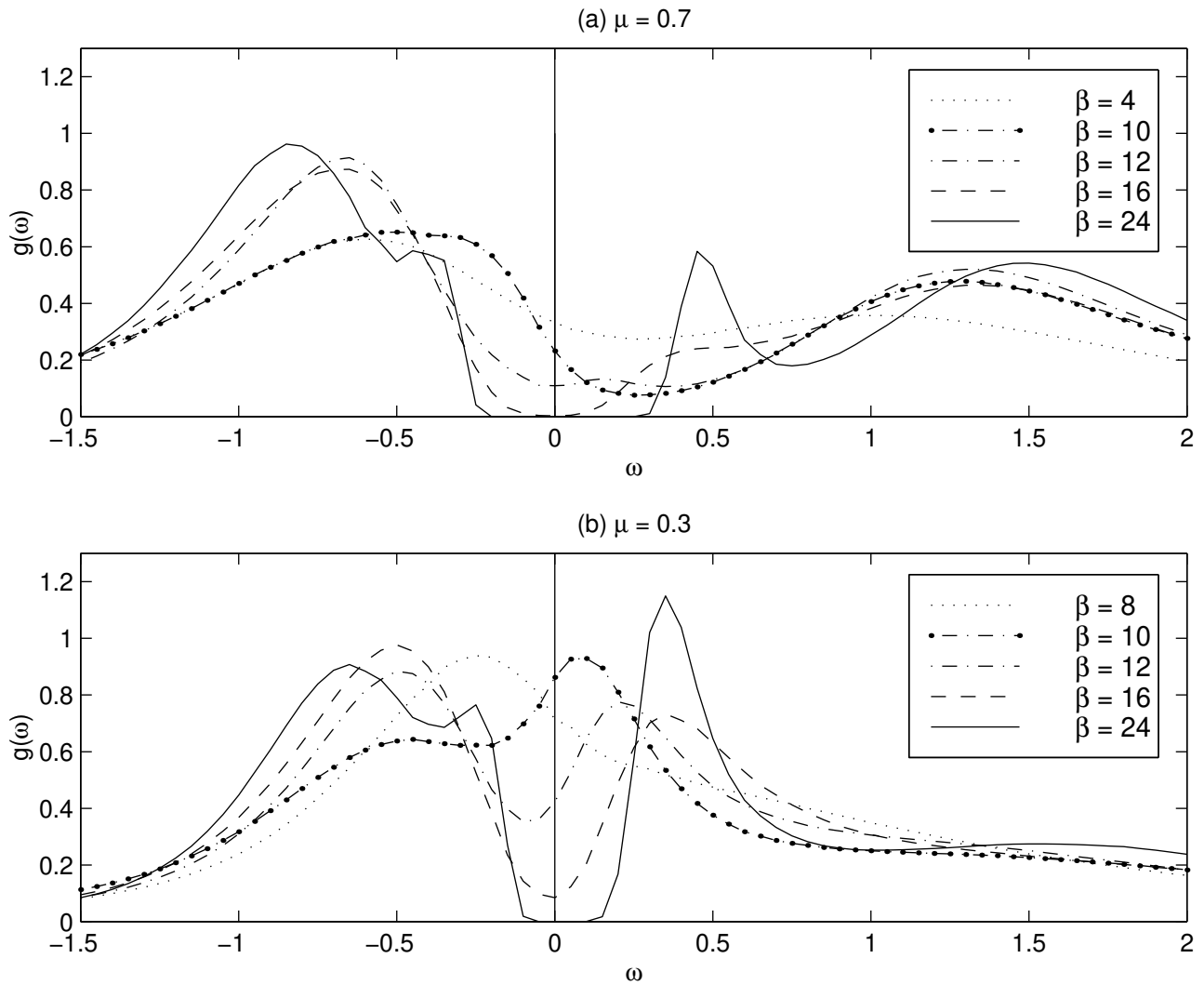


Figure 4 : Evolution of single-particle spectra as a function of temperature with inter-cluster anomalous terms. (a) is for small doping ($\mu = 0.04$) and (b) for large doping ($\mu = 0.17$).

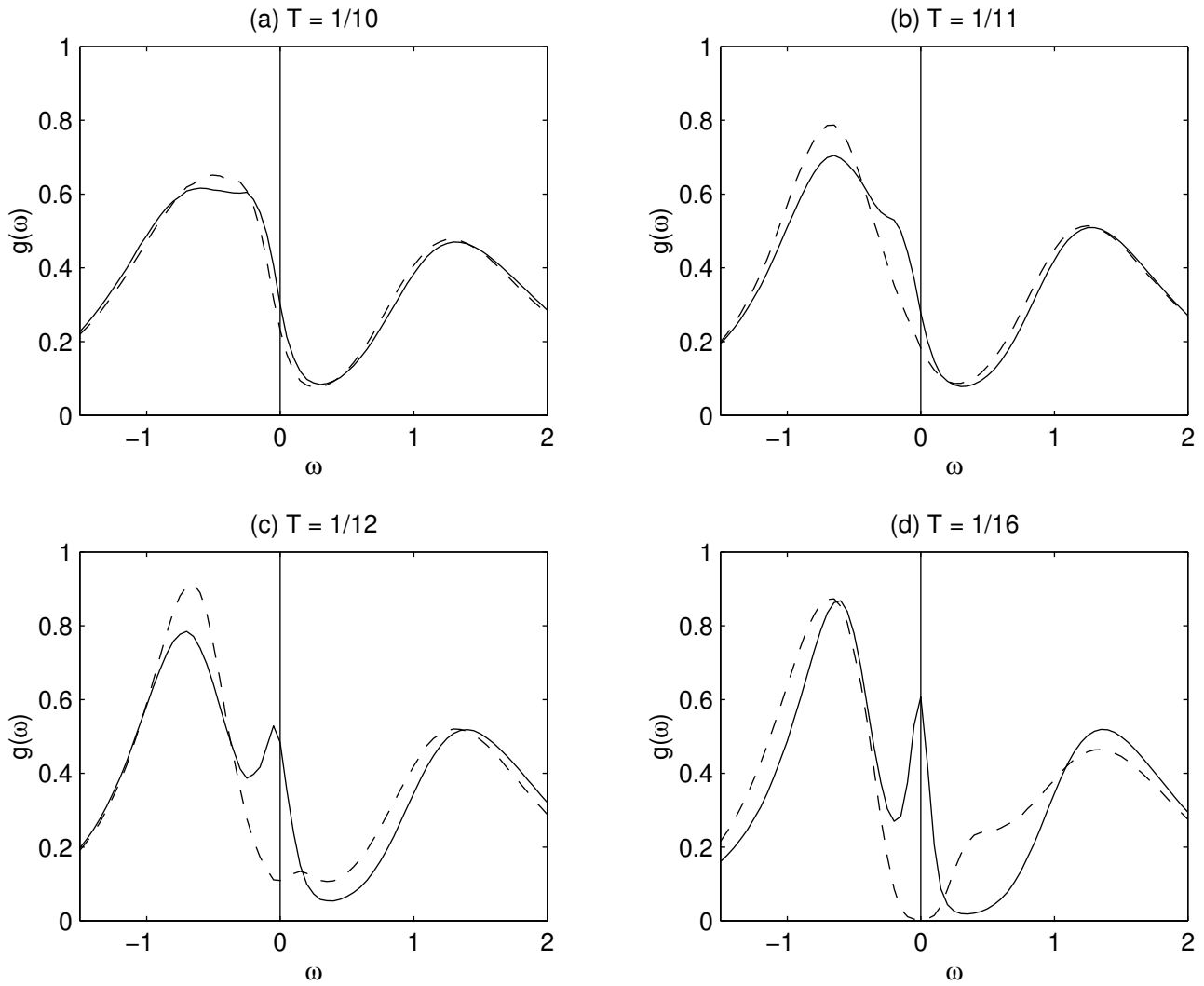


Figure 5 : DOS of normal(solid line) and SC (dashed line) state for $\mu = 0.7$ as a function of temperature. A gap feature clearly builds up as the superconducting correlation develops.

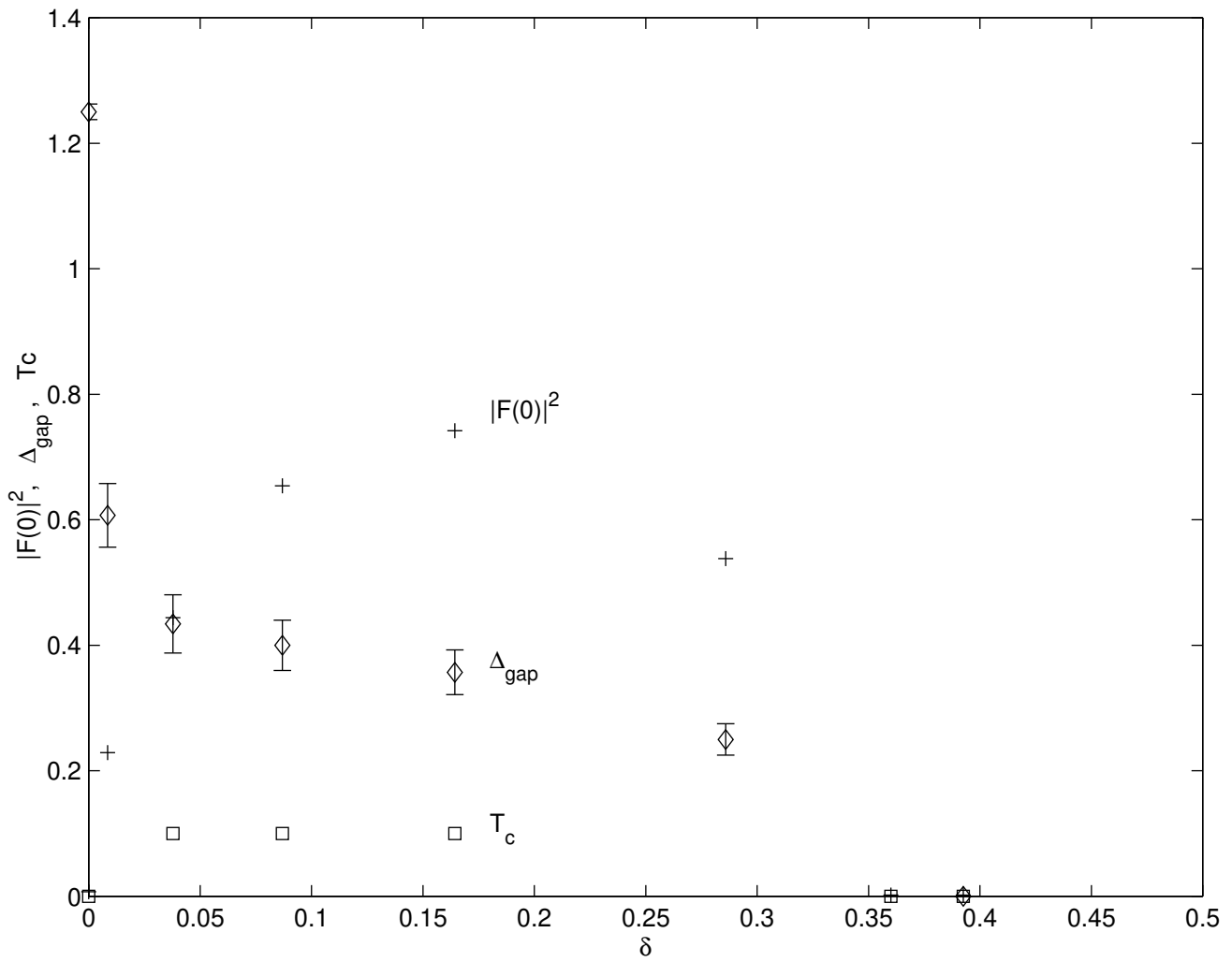


Figure 6 : A single-particle gap (diamond), Cooper pair density ($|F(0)|^2$, cross) and T_c (square) vs. doping at $t = 16$. Vertical units are arbitrary.

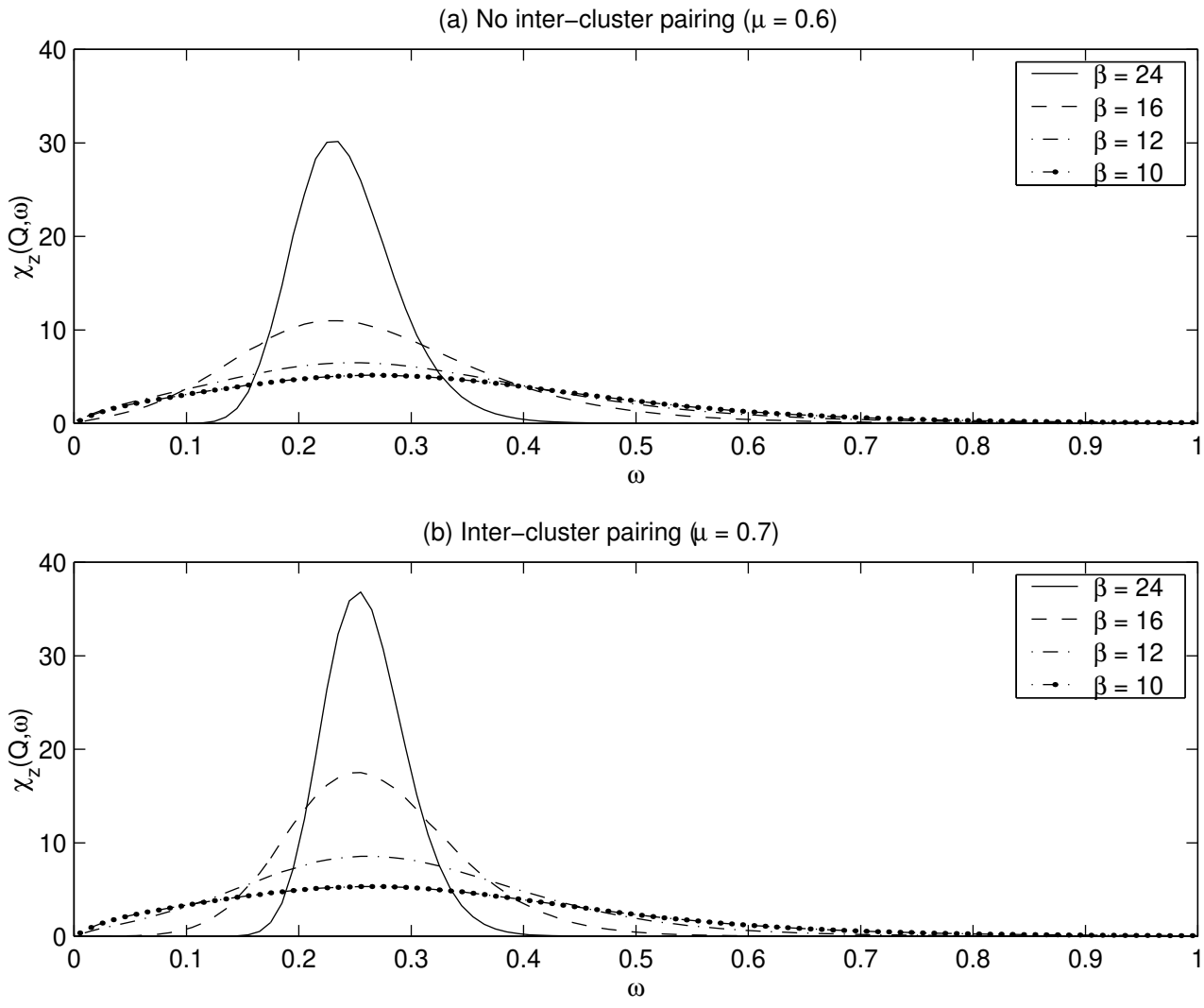


Figure 7 : $\chi_z(Q; \omega)$ as a function of temperature for the underdoped region. (a) without inter-cluster pairing and (b) with inter-cluster pairing.

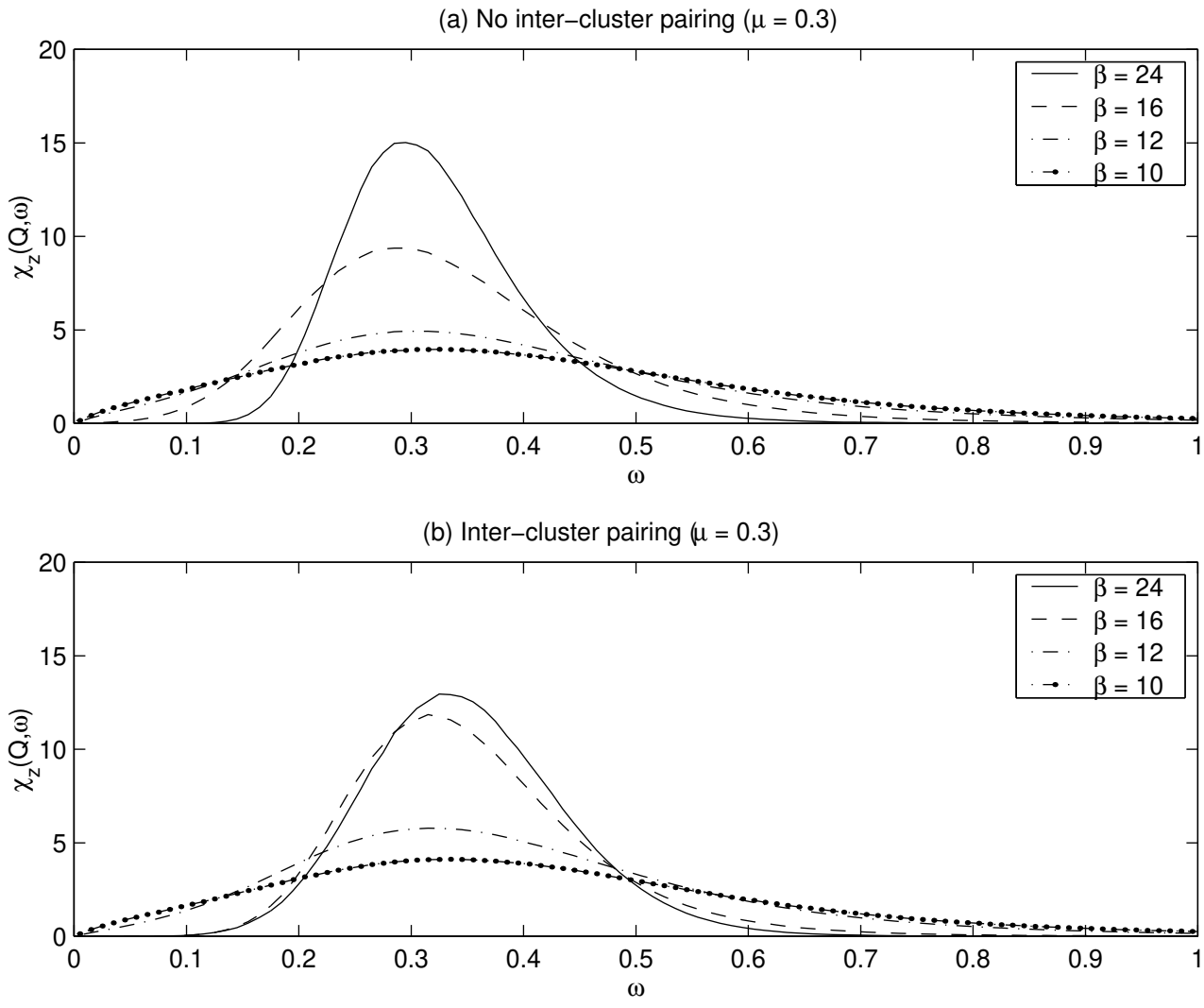


Figure 8 : $\chi_z(Q, \omega)$ as a function of temperature near optimal doping region. (a) without inter-cluster pairing and (b) with inter-cluster pairing.

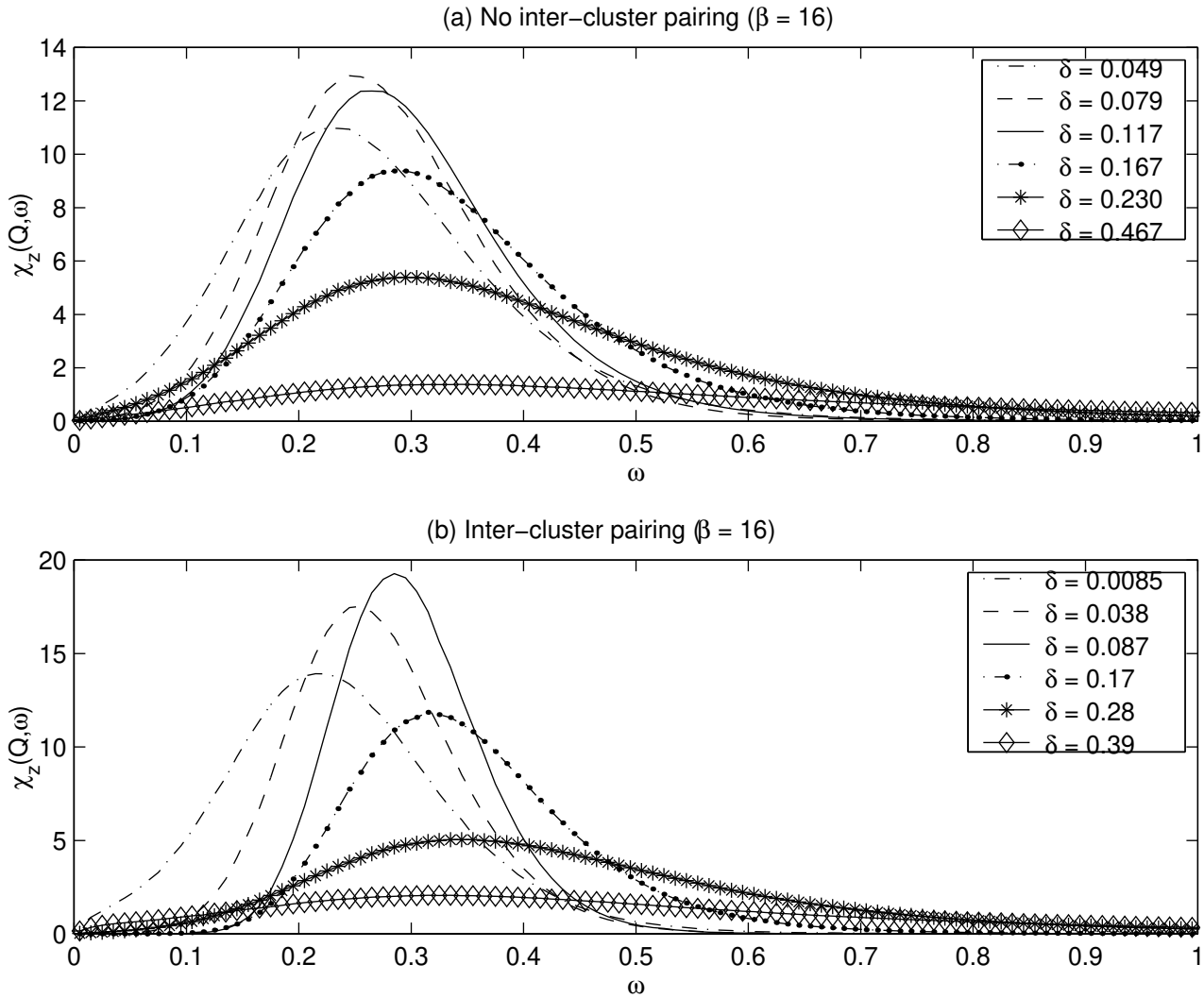


Figure 9 : $\chi_z(Q, \omega)$ as a function of doping. (a) without inter-cluster pairing and (b) with inter-cluster pairing.

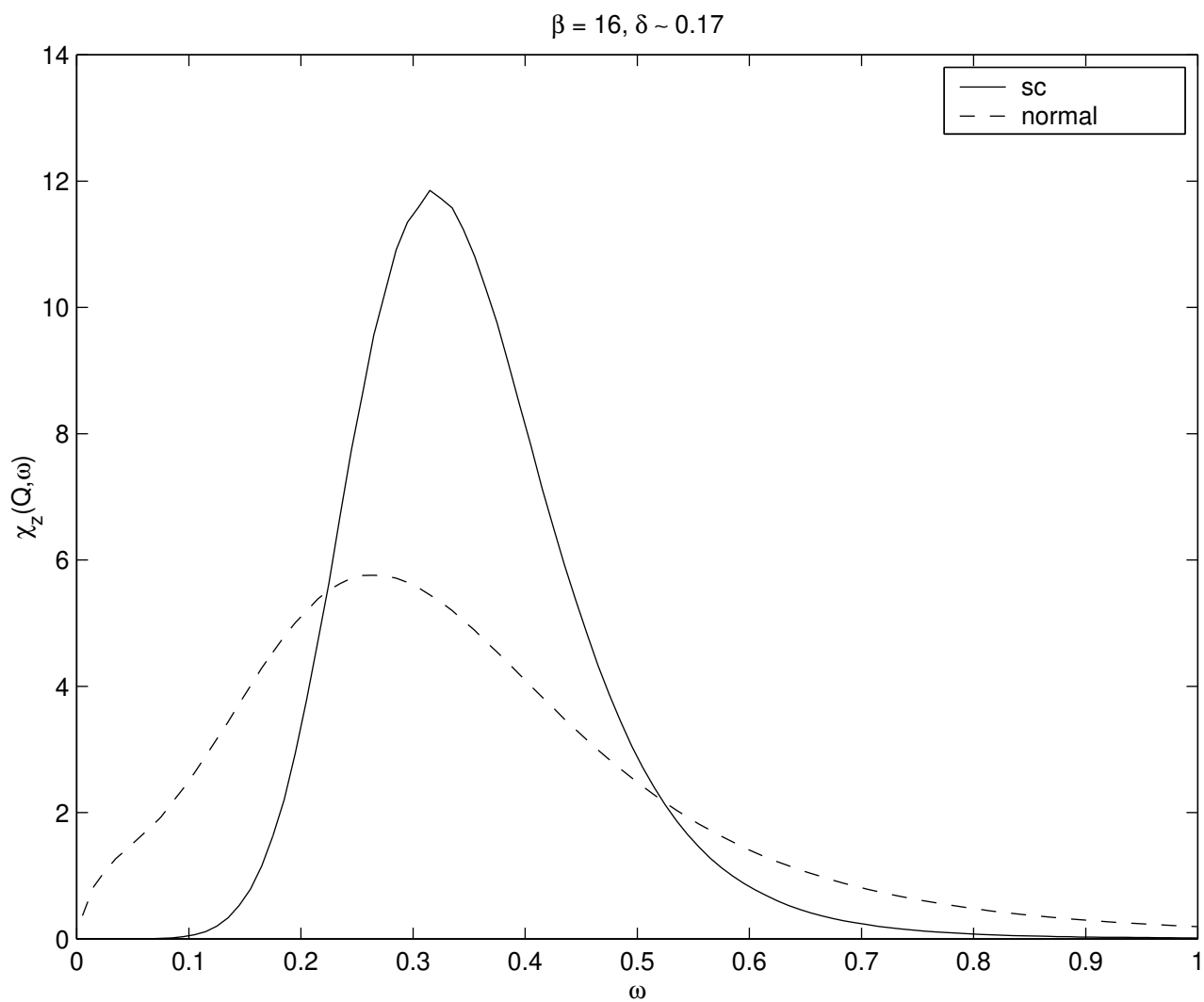


Figure 10 : $\chi_z(Q, \omega)$ spectra of normal (dash line) and SC (solid line) for $\beta = 16$ and $\delta = 0.3$. Coherence is severely degraded and the gap is filled in the normal phase.

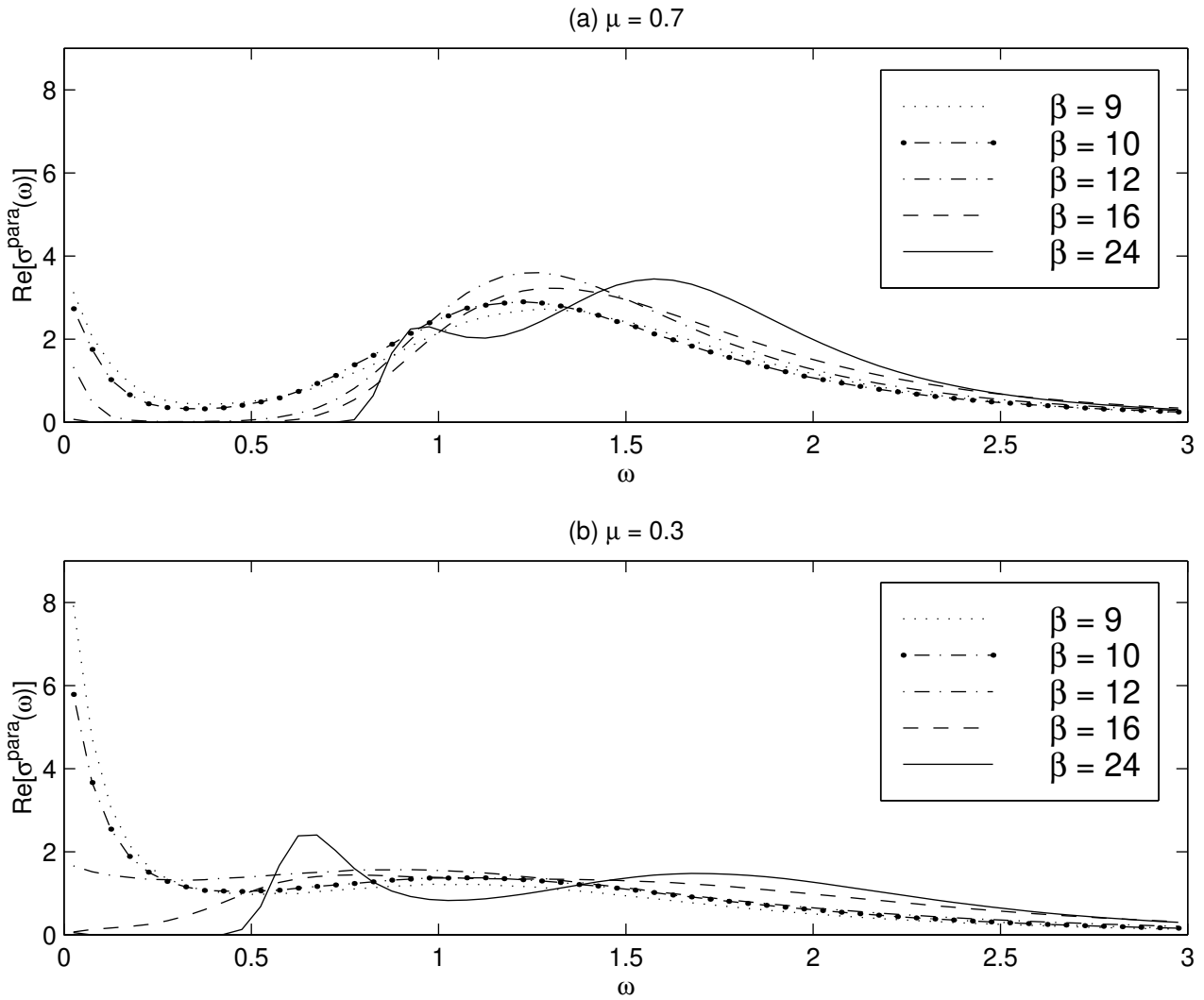


Figure 11 : $\text{Re}[\sigma^{\text{para}}(\omega)]$ as a function of temperature for $\mu = 0.7$ (a) and $\mu = 0.3$ (b). The horizontal unit is $2t$ and the vertical unit is arbitrary.

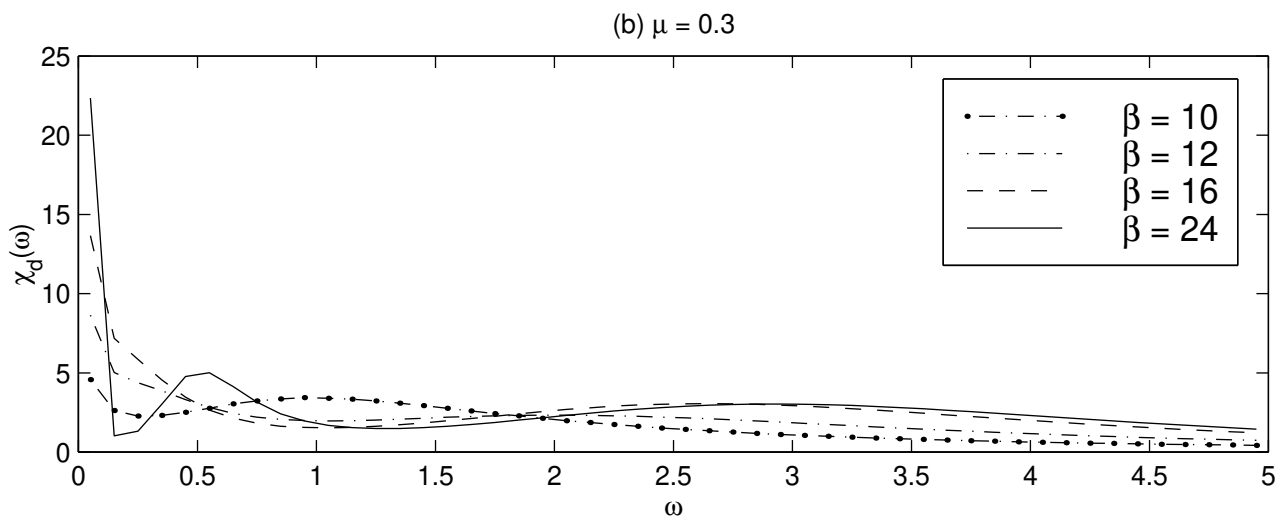
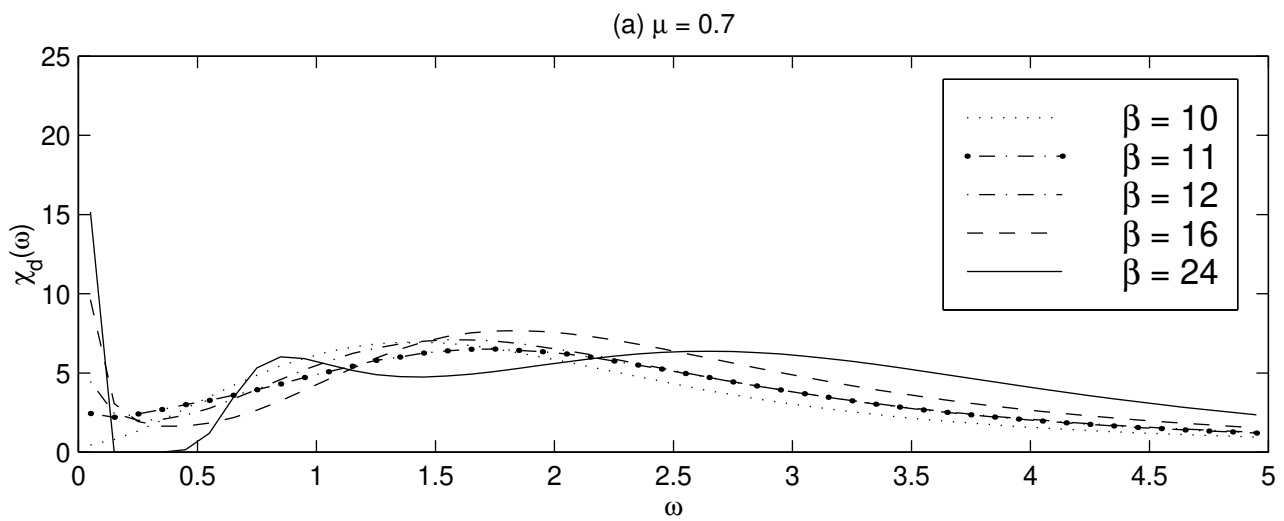


Figure 12 : $\chi_d(\omega)$ as a function of temperature for $\mu = 0.7$ (a) and $\mu = 0.3$ (b). The horizontal unit is $2t$ and the vertical unit is arbitrary.

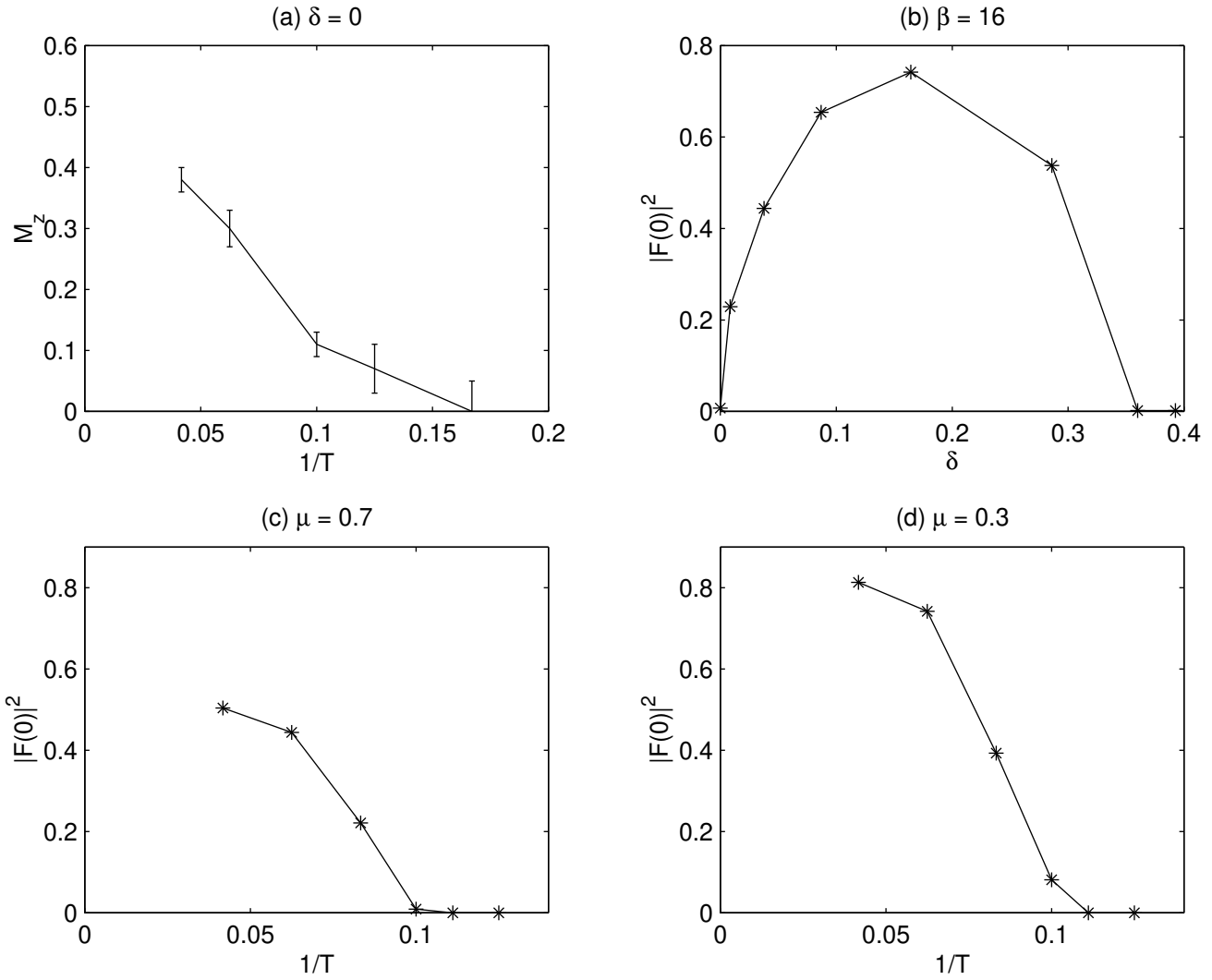


Figure 13 : (a) M_z vs. temperature at half filling. Units are μ_B and $2t$ for vertical and horizontal axis, respectively. (b) $|F(0)|^2$ vs. doping at $\beta = 16$. A unit for the vertical axis is arbitrary. (c) $|F(0)|^2$ vs. temperature for $\mu = 0.7$ (c) and $\mu = 0.3$ (d).

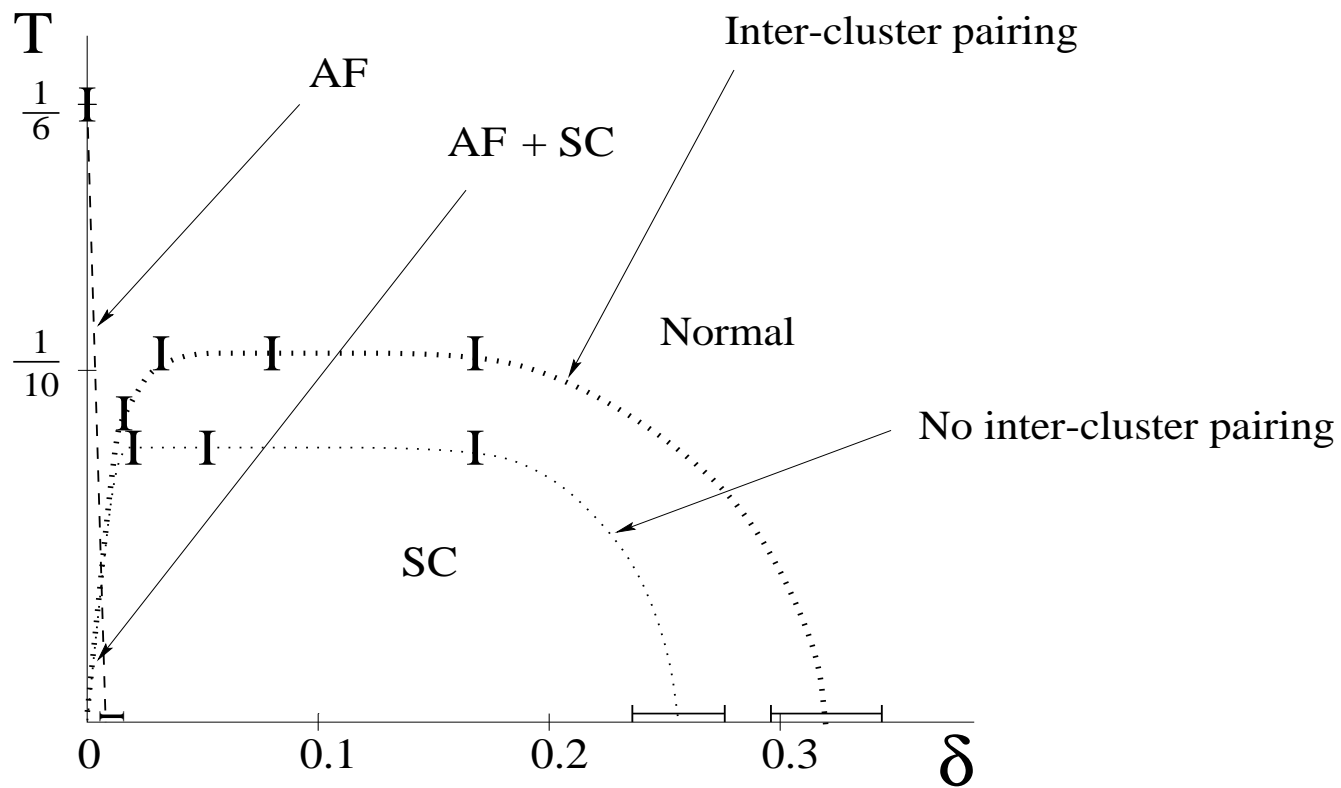


Figure 14 :Schematic phase diagram obtained based on our model. The onset of SC was determined by the appearance of a thermal average of an instantaneous pairing amplitude. Error bars correspond to the size of increments of sampling points we studied.